



Cite this: *Biomater. Sci.*, 2018, **6**, 726

Recent advancements in biocompatible inorganic nanoparticles towards biomedical applications

Mingxia Jiao,^{a,b} Peisen Zhang,^{a,c} Junli Meng,^{a,c} Yingying Li,^{a,c} Chunyan Liu,^{*a} Xiliang Luo^{ID}^b and Mingyuan Gao^{ID}^{*a}

Due to their intrinsic physical properties potentially useful for imaging and therapy as well as their highly engineerable surface, biocompatible inorganic nanoparticles offer novel platforms to develop advanced diagnostic and therapeutic agents for improved detection and more efficacious treatment of major diseases. The *in vivo* application of inorganic nanoparticles was demonstrated more than two decades ago, however it turns out to be very complicated as nanomaterials exhibit much more sophisticated pharmacokinetic properties than conventional drugs. In this review, we first discuss the *in vivo* behavior of inorganic nanoparticles after systematic administration, including the basic requirements for nanoparticles to be used *in vivo*, the impact of the particles' physicochemical properties on their pharmacokinetics, and the effects of the protein corona formed across the nano–bio interface. Next, we summarize the state-of-the-art of the preparation of biocompatible inorganic nanoparticles and bioconjugation strategies for obtaining target-specific nanoprobes. Then, the advancements in sensitive tumor imaging towards diagnosis and visualization of the abnormal signatures in the tumor microenvironment, together with recent studies on atherosclerosis imaging are highlighted. Finally, the future challenges and the potential for inorganic nanoparticles to be translated into clinical applications are discussed.

Received 9th November 2017,
Accepted 14th December 2017

DOI: 10.1039/c7bm01020f

rsc.li/biomaterials-science

^aKey Laboratory of Colloid, Interface and Chemical Thermodynamics, Institute of Chemistry, Chinese Academy of Sciences, Bei Yi Jie 2, Zhong Guan Cun, Beijing 100190, China. E-mail: gaomy@iccas.ac.cn, liuchy@iccas.ac.cn

^bKey Laboratory of Sensor Analysis of Tumor Marker, Ministry of Education, College of Chemistry and Molecular Engineering, Qingdao University of Science and Technology, Qingdao 266042, China

^cSchool of Chemistry and Chemical Engineering, University of Chinese Academy of Sciences, Beijing 100049, P. R. China

1. Introduction

The past decade has witnessed rapid advancements in nanotechnology and wide applications of nanoparticles (NPs, generally defined as particles ≤ 100 nm in diameter) in a variety of areas including materials science, energy, and medicine.^{1–7} In particular, inorganic NPs including iron oxide NPs, gold NPs, quantum dots (QDs) and rare earth NPs, which possess intrinsic magnetic, optical and electrical properties, are opening the



Mingxia Jiao

Dr Mingxia Jiao is a post-doctoral fellow in chemistry at the College of Chemistry and Molecular Engineering, Qingdao University of Science and Technology. She received her Ph.D. in physical chemistry (2016) from the Institute of Chemistry, Chinese Academy of Sciences (ICCAS) under the supervision of Prof. Mingyuan Gao. Her major research focuses on the synthesis and biomedical applications of multifunctional inorganic NPs.



Chunyan Liu

Dr Chunyan Liu is an associate professor in ICCAS. She received her B.Sc. in Chemistry from Xiamen University (2007), and received her Ph.D. (2013) in Physical Chemistry under the supervision of Prof. Mingyuan Gao in ICCAS. Her major research focuses on the synthesis and biomedical applications of nanomaterials.

way for developing advanced technology within the biomedical field.^{8–11}

One of the two major attractions for applying inorganic NPs in biomedicine is that their intrinsic physical properties, *e.g.*, superparamagnetism of magnetic NPs,^{4,12–14} surface plasmon resonance of metal NPs,^{15–17} luminescence of quantum dots^{18–20} and upconversion luminescence (UCL) NPs,^{8,21,22} can be tuned by engineering the size, shape, composition, and structure of the inorganic core for creating sensitive imaging or effective therapy. The other conspicuous attraction arises from the large surface-to-volume ratio of NPs, which not only allows for suitable decoration of the NP surface to regulate their *in vivo* behavior, but also offers multiple surface binding sites enabling NPs combining active targeting imaging and therapy.^{2,23–25} On account of these features, NPs can serve as an excellent platform for developing multifunctional theranostic nanovehicles and eventually realizing “precision medicine” and “personalized medicine”.

In fact, there already exist some inorganic NP-based agents which have been clinically approved, such as iron oxide NP-based ferumoxytol (Feraheme®), used to treat iron deficiency anemia in people with chronic kidney disease, and ferucarbotran (Resovist®), a magnetic resonance imaging (MRI) contrast agent for the detection and characterization of especially small focal liver lesions.²⁶ The promising pre-clinical results have also seen many inorganic NPs move rapidly to clinical trials recently, *e.g.*, Aurimmune CYT-6091 (phase II), an agent comprised of colloidal gold NPs bound with an immune-avoiding component (poly(ethylene glycol), PEG) and tumor necrosis factor (TNF) alpha for solid tumors.²⁵ However, the clinical translation of NP agents falls behind the fast development of the biological applications of NPs. The toxicity of NPs is an unavoidable aspect of concern for *in vivo* applications, but the main reason is that the *in vivo* behavior of NPs is rather complicated and affected by many parameters.^{10,27–29}

Previous investigations have revealed that the *in vivo* behavior of NPs is largely determined by the size, shape, composition, and the surface properties of NPs. Particularly, the surface properties including surface structure and charge,

hydrophilicity/hydrophobicity, and reactive moieties play an important role in nanomaterial cellular uptake, transport, and clearance.^{10,28,30–33} Once NPs are administered into blood, they have to first cross biological barriers and then accumulate in the target site.^{28,34} However, NPs are highly prone to interact across the nano–bio interface with proteins, lipids, and other biomolecules in the blood stream, leading to the formation of a dynamic “biomolecule corona” that influences the *in vivo* behavior of NPs.^{35,36} Therefore, a deep understanding of the nano–bio interface interplay between NPs and biological molecules will undeniably benefit the study of *in vivo* applications of NPs and further push their clinical translation.

In order to address these problems, various biocompatible surface modification strategies of inorganic NPs have been developed. Biocompatible polymers, such as PEG, poly(*N*-vinyl-2-pyrrolidone) (PVP), polysaccharides, polyacrylamide, and poly(vinyl alcohol), are most commonly used to decorate NPs for providing stealth characteristics to reduce or avoid non-specific interactions with opsonin proteins and uptake by the reticulo endothelial system (RES), thus resulting in longer blood half-life to help NPs accumulate in the site of interest.^{37–39} Other strategies have also emerged such as zwitterionic coating, and bio-inspired coating to obtain highly biocompatible NPs for *in vivo* imaging and therapy.^{25,40,41} Meanwhile, on the basis of this surface engineering, targeted nanoprobe, and intelligent and stimuli-responsive probes are also being developed to improve the efficacy of diagnosis and treatment.^{30,41–43}

To date, numerous attempts have been focused on controllable synthesis, surface modification of inorganic NPs, and biomedical imaging and therapy based on biocompatible NPs. Opportunities and challenges exist side by side with the nanotechnology and nanomedicine advancing rapidly. In the current review, we will provide an in-depth insight into how the factors influence the *in vivo* behavior of NPs, followed by the classical and novel surface coating strategies through *in situ* synthesis or post modification of inorganic NPs represented by iron oxide, gold, semiconductor, and UCL NPs, and then briefly summarize the bioconjugating strategies and state-of-the-art in *in vivo* imaging applications of NPs including active targeted tumor imaging and tumor microenvironment responsive imaging as well as atherosclerosis imaging in recent years.



Mingyuan Gao

Prof. Mingyuan Gao is a Full Professor in ICCAS. He received his BSc (1989) and PhD (1995) in Polymer Chemistry and Physics at Jilin University. He worked as a research assistant and associate in Germany from 1996 to 2002 and was an A. v. Humboldt fellow between 1996 and 1998. His research focuses on the synthesis as well as biological and biomedical applications of functional nanomaterials.

2. *In vivo* behaviors of inorganic NPs

The increasing biomedical applications for both diagnostic and therapeutic purposes inspire the comprehensive understanding of the *in vivo* behavior of inorganic NPs. Even though the toxicity of inorganic NPs is a matter of concern among researchers for *in vivo* applications all the time, it's still far from conclusive and consensus. Yet the superiority of NPs in biomedical fields promotes the fast development of nanomedicine. Previous reviews have summarized NP toxicity, which help to understand their biological effects.^{28,44–50} When

NPs enter the physiological environment, the physicochemical properties or the integrity of NPs could be changed dramatically following protein binding, internalization by cells and degradation, which would inevitably influence the *in vivo* behavior of NPs. Herein, we'll focus on the *in vivo* behavior and interactions between NPs and biological factors.

2.1 Basic requirements for biomedical applications

For *in vivo* theranostic applications, inorganic NPs are generally required to possess basic properties including water solubility and colloidal stability under physiological conditions, apart from bearing the desired physical properties. Generally, hydrophobic NPs are poorly dispersed in biological fluids, and tend to form aggregates due to the hydrophobic interaction, thus altering their physicochemical properties. Therefore, the water solubility and colloidal stability under physiological conditions are the first requirement for *in vivo* applications. Meanwhile, the physical properties of NPs are expected to be steady in the circulating system after the particles are administered into the body. For example, the fluorescent stability of QDs needs to maintain within the complex physiological environments to provide accurate physiological or pathological processes related to optical signals.

Biocompatibility is the most important prerequisite for inorganic NPs being used *in vivo*. The biocompatibility of a material refers to its ability to perform its desired function in a medical therapy without eliciting any undesirable local or systemic effects in the recipient of that therapy, but generating the most appropriate beneficial cellular or tissue response in that specific situation, and optimizing the clinically relevant performance of that therapy.¹ Since the administered NP-based agents are desired to be eliminated from the body after exerting their functions, the toxicities of both the inorganic core and coating materials, local or systemic effects, circulating behavior and elimination pathways are the major concerns towards biomedical applications. Biocompatible surface modification of NPs, on the one hand endows the NPs with water solubility, stability, and biocompatibility, on the other hand modulates the pharmacokinetics and medical functions of NPs aiming at different tissue or organ lesions. For instance, Bawendi *et al.* designed InAs-based QDs coating with three different ligands. Phospholipid micelle coated QDs allowed a long blood circulation time and thus enabled angiography and related applications such as vital sign monitoring. QDs incorporated into lipoproteins enabled imaging of the energy metabolism of activated tissues and organs in real time. Large QDs composite particles coating with both phospholipid and lipoprotein were bright enough for single particle tracking to generate large-scale three-dimensional blood flow maps for a quantitative description of local tissue microenvironments.⁵¹ In addition, in view of specific diagnosis and therapy, suitable surface functionalization is also an important aspect for establishing biological targeted nanoprobes.

Besides the above requirements, reproducible and large-scale production of high quality NPs is indispensable for their clinical translation, which raises great challenges in batch syn-

thesis. Fortunately, flow chemistry brings solutions to the poor batch-to-batch reproducibility, and provides the possibility for large scale production of first-class nanomaterials. Still, there is a long way to go for the NP-based agents to eventually live up to clinical use.

2.2 Pharmacokinetic behaviors of NPs

A comprehensive understanding of NPs' pharmacokinetic characteristics is of fundamental significance for their design, synthesis, and optimization for suitable risk assessment and safe and efficacious applications in the field of nanomedicine. Pharmacokinetic data can quantitatively reflect the exposure of organs and tissues to the NPs, which affects not only toxicity but also the targeting efficiency. The pharmacokinetic behaviors including biodistribution, blood half-life, and the clearance pathway of NPs are often a matter of concern in the *in vivo* applications. Taking tumor imaging as an example, since extravasation of NPs from tumor vasculature to extracellular tumor microenvironment could be considered as an accumulative process, the long half-life and high concentration of NPs in blood are favorable for enhancing the uptake of NPs into the tumor site, which improves tumor targeting efficiency. In general, the pharmacokinetic behaviors of inorganic NPs are largely dominated by their hydrodynamic size and surface properties including surface structure and charge, and conjugated moieties.

2.2.1 Effect of particle size. The particle hydrodynamic (HD) size, which is determined by both the inorganic core size and the surface coating, has a tremendous impact on the uptake and clearance routes of NPs.^{52,53} Generally, particulate matter with a HD size larger than approximately 100 nm would be rapidly sequestered by the RES also known as the mononuclear phagocytic system (MPS), functionalizing through monocytes circulating in the blood, dendritic cells and macrophages present in the liver, spleen, lung, and bone marrow.²⁵ In contrast, particles with a HD size of around 5.5 nm or less are able to pass through the pores of the glomerulus in the kidney, *i.e.*, rapidly cleared *via* renal filtration. For instance, it was found that more than 50% of neutrally charged 2 nm glutathione (GSH)-coated Au NPs were excreted through urine within 24 h after intravenous injection,⁵⁴ and 5.5 nm PVP-coated CuS nanodots could pass through the barrier for efficient renal clearance and displayed substantially less liver and spleen uptake than that of 32 nm PEG-coated CuS NPs.⁵² For the particles with a HD size between 5.5 and 100 nm, the blood half-life and biodistribution also vary along with the particle size. For example, 45 nm PEG-coated Au NPs were demonstrated to have prolonged blood circulation time and reduced uptake by the liver and spleen compared with 90 nm PEGylated Au NPs, most of which were rapidly taken up by the RES.⁵⁵ Similar results were obtained by the biodistribution studies on the 6 nm and 13 nm GSH-coated Au NPs which show that over 40% of the 13 nm particles *vs.* only 4% of the 6 nm particles were observed in the liver.⁵⁴

Although rapid clearance of NPs from the body may reduce the concern of influence of NPs on the organs, sufficiently

long blood half time is desired for enhancing the chance of NPs to accumulate in the targeted site. Gao's group reported a dramatic size-dependent photoacoustic (PA) imaging of tumors based on PEGylated copper sulfide NPs.⁵⁶ Three differently sized NPs were aqueously synthesized, *i.e.*, 2.7 nm, 4.8 nm, and 7.2 nm, with HD sizes of 7.1 nm, 10.7 nm, and 14.9 nm respectively, and exhibited satisfying colloidal stability both in water and PBS. The blood half time was found to be inversely proportional to the particle size. As expected, the smaller particles presented a better PA contrast enhancement effect for tumor imaging *in vivo*. On the other hand, the change of NPs' biodistribution can reveal the different clearance pathways. Liu *et al.* carefully studied the size-dependent pharmacokinetic behavior of PEGylated NaGdF₄ particles, *i.e.*, 18.5 nm and 5.1 nm (core size).³¹ As shown in Fig. 1, two NPs presented a similar biodistribution with a little higher liver uptake for the larger particles. Nevertheless, the detailed quantitative analysis revealed that the smaller particle exhibited a longer blood half time, *i.e.*, 178 min *vs.* 66 min, but a shorter biological half time, *i.e.*, 1.4 days *vs.* 7.0 days, which suggested that these two particle samples may take different elimination pathways. Further systematic investigations suggested that the renal clearance was one of the major elimination pathways for the 5.1 nm particle, while the biliary clearance acted as the major elimination pathway for the larger one, although it was taken by both particles. Excitingly, the large particles found in the feces collected on the 3rd and 14th day post injection presented no differences in size, size distribution, and shape, compared with the mother particle, which helped to relieve

the concerns on the toxicity of the NaGdF₄ particles due to the possible eroding within the body.

2.2.2 Effect of the surface structure. The surface structure of inorganic NPs determined by the type and density of decoration molecules dominates the *in vivo* behaviors of NPs, manifesting as direct control over the interface interaction between NPs and the biological systems. The interplay of NPs and proteins will be discussed in the next section. A suitable design of the surface structure can maximize therapeutic or diagnostic efficacy while minimizing unfavorable side effects.

As is known, NPs have large specific surface area and high surface energy, and thus tend to interact with the abundant biomolecules within the body.¹⁰ In order to reduce the nonspecific adsorption of serum proteins onto the particle surface, surface modification tactics are popular in achieving biocompatible NPs, endowing the stealth nature of the nanoparticles, which means evading uptake by the RES organs and thus prolonging the blood circulation time.^{57,58} Different decoration molecules bring about distinct functions for modulating the surface structure of NPs so as to affect their *in vivo* behavior. For example, PEG is a typical biocompatible molecule for effectively overcoming the nonspecific adsorption of proteins, and the chain length appears to influence the pharmacokinetics of NPs. Choi *et al.* reported an organ/tissue selective biodistribution and elimination of near-infrared (NIR) fluorescent InAs@ZnS QDs which were coated with a systematically increasing chain length of dihydrolipoic acid (DHLA)-PEG.⁵⁹ QDs coated with a shorter PEG chain length, *i.e.*, PEG₃ (3 repeating units, HD size of 5.3 nm) and PEG₄ (HD size of 5.6 nm), exhibited rapid renal clearance. In contrast, a bit longer chain length (PEG₈, HD size of 6.5 nm) resulted in the excretion of the particles through the liver and bile, and quite surprisingly, preferential accumulation in the parenchyma of the pancreas. Along with a further increase in the PEG chain length (PEG₁₄, HD size of 8.7 nm), the blood half time of the QDs increased significantly up to 922 min, rendering the QDs more likely subjected to hepatic clearance and uptake in lymph nodes.

Apart from PEG, biomolecules such as zwitterionic GSH,^{57,60} bovine serum albumin (BSA),⁶¹ human serum albumin (HSA),¹⁹ cell membrane,⁶² and self-peptide³⁰ can also help resist the harvesting of RES but result in different effects on the pharmacokinetics of NPs. For example, Zheng and co-workers prepared two renal-clearable Au NPs with almost identical photophysical properties, core sizes, low affinity to serum protein, high physiological stability and slightly different HD sizes (5.5 nm *vs.* 3.3 nm), *i.e.*, PEG1000-Au NPs and GSH-Au NPs, and compared the ligand effect on renal clearance and passive tumor targeting.⁵⁷ Renal clearance kinetics revealed that the amount of GSH-Au NPs excreted through urine rapidly reached its maximum within 1 h post injection, while it took five hours for the PEGylated particles. Systematic studies showed that the PEG-Au NPs could target tumors with an efficiency three times higher than that of the GSH-Au NPs, although both particles exhibited comparable low RES uptake. This is fundamentally a result of the fact that PEGylation can

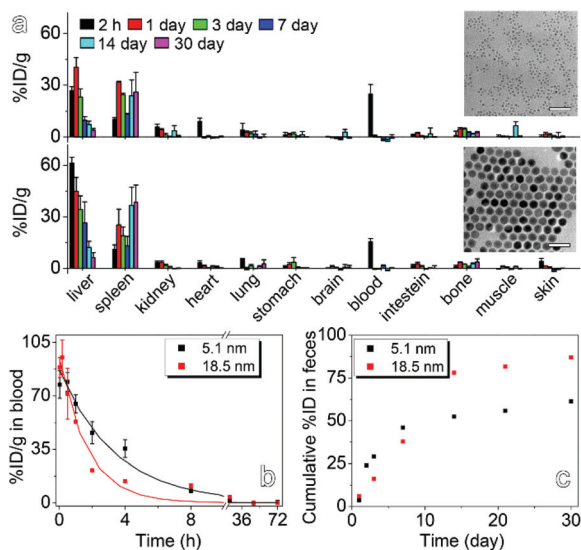


Fig. 1 (a) Biodistribution of intravenously injected NaGdF₄ particles (5.1 nm) and NaGdF₄:Yb,Er particles (18.5 nm) whose representative TEM images are shown as insets, together with the blood clearance profiles of the two particles in Kunming mice (b) and cumulative amounts of these two particle samples found in feces of mice at different time points post injection (c). All embedded scale bars correspond to 50 nm. Reproduced from ref. 31 with permission, copyright 2013, American Chemical Society.

effectively enhance the accumulation of NPs to the tumor site through increasing the blood half-life relative to zwitterionization. Chen and co-workers also found that compared with GSH- ^{64}Cu]CuInS/ZnS QDs, the PEGylated QDs showed more than two times higher tumor uptake to a maximum of 10.8% ID g^{-1} , although both QDs were largely accumulated in the liver and spleen at 48 h post injection.⁶⁰ Inspired by the “self-recognition” of the living system, Gao and coworkers adopted the self-peptide as the outermost surface layer of the diphosphate-PEG coated Fe_3O_4 tumor imaging nanoprobe for evading the RES uptake.³⁰ As shown in Fig. 2, the efficient stealth of the macrophage uptake was firstly demonstrated by *in vitro* experimental results. As expected, the self-peptide modification largely increased the blood half time to 8.2 h from 2.8 h for the mother PEGylated Fe_3O_4 NPs.

2.2.3 Effect of surface charge. The surface charge of inorganic NPs directly depends on the molecular structure of the coating materials. For instance, amine groups usually contribute to a positive charge on NPs, while a negative charge is expected for NPs with carboxyl and/or sulfate groups.⁶³ Surface charge affects the interaction of NPs with serum proteins and cell membranes as well, thus having non-ignorable influence on the pharmacokinetics and biodistribution of NPs.^{10,52,64–66} It is generally agreed that a neutral surface charge from zwitterionic or neutral coatings can effectively weaken unexpected serum protein adsorption, and thus would lead to a longer blood half-life. Arvizo *et al.* used a series of structurally consistent Au NPs (2 nm core/ 10 nm HD size) with

different surface charges, *i.e.*, negative (carboxyl group terminated, -37.9 mV), zwitterionic (quaternary ammonium and sulfate groups terminated, -2.0 mV), neutral (hydroxyl group terminated, -1.1 mV), and positive (quaternary ammonium group terminated, 24.4 mV), to quantify the role of surface charge on the pharmacokinetics, tumor uptake and biodistribution of Au NPs.⁶⁷ Neutral and zwitterionic NPs were demonstrated to exhibit a longer circulation time *via* both tail intravenous and intraperitoneal injections, whereas negatively and positively charged particles possess relatively short half-lives. These pharmacological characteristics were reflected on the enhanced tumor uptake for neutral and zwitterionic NPs *via* passive targeting. With respect to the metabolic pathway, surface charge was demonstrated to affect whether the NPs can be degraded through renal clearance by Choi *et al.*⁶⁸ It was verified that upon zwitterionic or neutral coatings, CdSe/ZnS QDs could be eliminated from the body by rapid and efficient urinary excretion due to the HD size smaller than 5.5 nm. Conversely, negative or positive coating resulted in the HD size to be increased from 3 nm up to 15 nm or more *via* protein adsorption, leading to the renal non-removable QDs which mainly accumulated in the liver, lung, and spleen. Nevertheless, even when the HD size is below 5.5 nm, the NPs can still not be eliminated by the kidney if possessing unsuitable surface charge. Liang *et al.* found that the negatively charged CdTe/CdS QDs with a HD size of 3.7 nm were lack of urinary excretion due to the barrier of the anionic glomerular basement membrane, rather than the increased HD size caused by protein binding, because the same type of QDs (HD size of 5.6 nm) with positive surface charge did show quick renal clearance after administration.⁶⁹ This result strongly emphasizes the impact of surface charge on the renal excretion of inorganic NPs.

Apart from the particle size, surface structure and charge, other factors including NPs' shape,¹⁶ the mode and dose of systemic administration,⁷⁰ *etc.*, can also uniquely alter the pharmacokinetics, and the uptake of inorganic NPs in the targeted site. Despite the remarkable progress, enormous challenges still exist in uncovering how the above parameters individually affect the pharmacokinetic behavior of inorganic NPs, because it is technically difficult to maintain all the other parameters the same and compare the influences only based on one parameter.⁶³ Therefore, precise control over the construction of NP-based agents from the inorganic core to surface coating needs to be further improved to promote the clinical translation of NPs.

2.3 The nano-bio interface

Towards *in vivo* diagnostic or therapeutic applications, NPs are usually introduced into the biological environments such as blood, at which point they are exposed to highly complex surroundings containing a plethora of ions and biomolecules such as lipids, sugars, and especially proteins.^{28,35,71} In this context, they will inevitably adsorb onto the surface of the NPs, mediated by van der Waals, electrostatic, hydrogen bonding, and/or hydrophilic/hydrophobic interactions. The sum of all

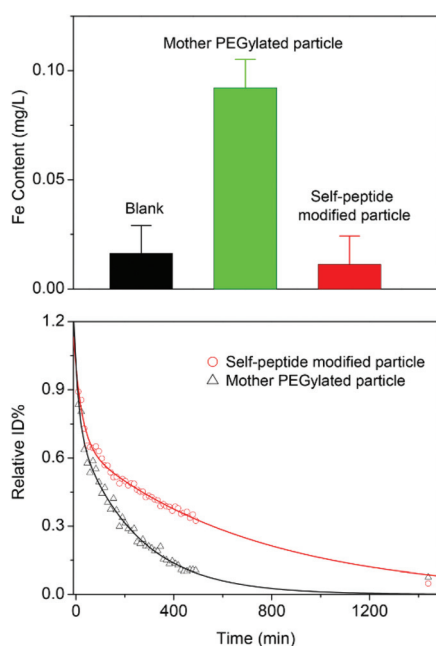


Fig. 2 Fe content in RAW264.7 cells treated with the mother PEGylated Fe_3O_4 nanoparticles and the self-peptide modified particles respectively (blank represents untreated cells), and the blood residence profiles of the two particles in nude mice overlaid with two-compartment fitting curves for extracting the blood half-lives of the particles. Reproduced from ref. 30 with permission, copyright 2017, Wiley-VCH.

adsorption processes across the nano–bio interface will result in the unintended formation of the so-called “biomolecule corona”, of which the “protein corona” has been studied the most so far.²⁸ It's of great significance to consider the further biointeraction and biomodification of NPs in biological environments, which may adversely impact their final utility.

The protein corona formed in the body is far more complex than *in vitro* trials due to the complex environment (nearly 2000 different proteins in widely varying concentrations) and dynamic processes of corona formation.³⁵ Proteins involved in both physiological and pathophysiological relevant processes have been identified in the coronas of various NPs.⁴ The protein corona not only influences the adhesion to the cell membrane and subsequent internalization of NPs, but also has a severe effect on the physicochemical properties of NPs and further on their pharmacokinetic behavior.¹⁰ The formed protein corona may trigger the transformation of NPs by altering their colloidal stability, either exhibiting a stabilizing effect by inducing steric stabilization or destabilizing impact caused by protein mediated bridging, charge compensation or the introduction of charge inhomogeneity onto the NP surface.⁷² For example, Gao *et al.* found that both negatively and positively charged iron oxide NPs lose their colloidal stabilities when exposed to plasma proteins including serum albumin and immunoglobulin G (IgG).²⁵ Moreover, the HD size of NPs with the corona was dramatically increased, which would accelerate the macrophage uptake of the NPs into the liver, spleen, and bone marrow in the RES system. In addition, binding of opsonins such as IgG and complementary factors could promote the clearance.⁷³ Such an accumulation of the opsonized NPs into the RES organs is considered to be favorable when these organs are the intended target sites. However, for delivering the inorganic NPs to tissues other than the RES organs, the accumulation of NPs would lead to tissue toxicity as well as low theranostic efficiency by losing the targeting ability, and therefore in this context minimizing the opsonization of protein to NPs becomes essential.

Currently, the protein corona is far from being understood and still remains unpredictable, therefore, attempts to partially or even completely prevent protein adsorption are persistently investigated, although some proteins in the corona present a positive effect on the theranostic represented by apolipoprotein which can promote the movement of nanoprobe across the blood brain barrier.⁴ The appropriate surface engineering of NPs, which dominates their interaction with plasma proteins, should be pursued for preparing stealth NPs or “corona-free” NPs.

3. Synthetic strategies of biocompatible NPs

Wet-chemical synthesis techniques provide a reliable way to prepare diversified inorganic NPs with high quality, on the basis of which biocompatible NPs for biomedical applications

can be obtained *via in situ* “one-pot” synthesis of hydrophilic particles or post surface modification of hydrophobic NPs.

3.1 *In situ* coatings via “one-pot” synthesis

Aqueous synthesis is in principle the simplest method to prepare water dispersible NPs, which can commonly be obtained in the presence of hydrophilic ligand molecules.^{3,24} Small molecules bearing chelating groups like carboxylic, thiol, and amine groups, such as citric acid, tartaric acid, mercaptoacetic acid, dimercaptosuccinic acid, phosphoryl choline, and GSH, can bind onto the particle surface as well as the precursor or monomer surface to stabilize and regulate the formation of NPs.¹ For instance, aqueous synthesis has long been used to grow QDs including CdTe, CdSe, and CdS, involving mixing of cadmium precursors in the presence of thioalkyl acids or amines in aqueous solutions followed by the injection of tellurium, selenium, or sulfur precursors.^{3,74} In addition, biopolymers such as carbohydrates (dextran, chitosan, alginate, and arabinogalactan), proteins such as lipoproteins, as well as synthetic polymers such as PEG, poly(acrylic acid) (PAA), poly(methacrylic acid) (PMAA), PVP, and polyethylenimine (PEI), are often used as biocompatible ligands in the aqueous synthesis.^{1,24,39,56} One representative example is an MRI contrast agent Feridex, *i.e.*, superparamagnetic iron oxide NPs coated with dextran, which shows good biocompatibility for FDA-approved clinical use.²⁶

Although biocompatibility can be achieved by aqueous synthesis, the properties of the resulting NPs are often unsatisfactory, *e.g.*, the quantum yield of QDs tends to be relatively lower than those prepared through non-hydrolytic synthetic routes, and the iron oxide NPs synthesized by the co-precipitation method show broad size distribution and low saturation magnetization. For developing biocompatible high quality magnetic NPs, Gao's group pioneered a novel “one-pot” approach by using a carboxylated PEG ligand for *in situ* coating the iron oxide core during the synthetic process through thermally decomposing Fe(acac)₃ as shown in Fig. 3.^{37,76} 2-Pyrrolidone was firstly used as a high boiling point solvent to synthesize monodisperse iron oxide NPs in the presence of monocarboxyl-terminated PEG2000 (MPEG-COOH).³⁷ The resulting particles possess an excellent solubility in aqueous solution as well as in physiological saline, and the particle size can be tuned in a range of 4–10 nm by altering different reaction parameters such as the molar ratio of PEG and Fe(acac)₃, the molecular weight of PEG, and the concentration of Fe(acac)₃.^{37,75} The MRI results indicated that the developed “one-pot” synthetic approach opens up a new way for directly synthesizing magnetite NPs with very good biocompatibility and long blood circulation time which are potentially useful as MRI contrast agents.⁷⁵ Furthermore, by using α,ω -dicarboxyl-terminated PEG (HOOC-PEG-COOH) as a surface capping molecule instead of MPEG-COOH, magnetite NPs with surface reactive moieties were obtained, and used straightforwardly as effective MRI contrast agents in cancer diagnosis after conjugation with a

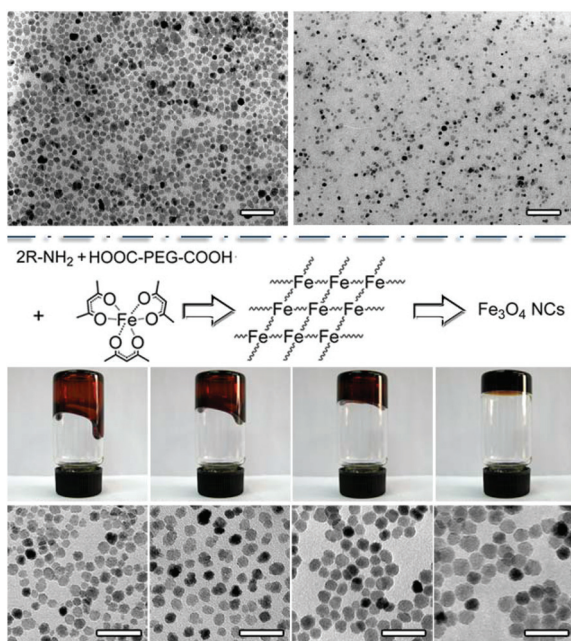


Fig. 3 The upper panel: the representative TEM images of MPEG-COOH and HOOC-PEG-COOH modified Fe_3O_4 NPs, respectively. The lower panel: a sketch of the gelification process for producing differently sized biocompatible Fe_3O_4 nanoparticles, together with the photographs of precursor solutions with different gelification degrees and representative TEM images. All embedded scale bars correspond to 50 nm. Reproduced from ref. 14, 37, 75 with permission, copyright 2005 and 2006, Wiley-VCH, and Copyright 2011, American Chemical Society, respectively.

specific cancer-targeting antibody.⁷⁶ In addition, the particle size was successfully tuned from 12 nm to 27 nm by increasing the precursor concentration while maintaining the monodispersity.

Since the iron oxide NPs costabilized by carboxylated PEG and 2-pyrrolidone were demonstrated by the same group to show obvious nonspecific adsorption of plasma proteins due to the positive surface potentials, diphenyl oxide, a non-coordinating high boiling point solvent, was used instead of 2-pyrrolidone to synthesize biocompatible Fe_3O_4 NPs in the presence of oleylamine and HOOC-PEG-COOH.^{14,77,78} The resulting NPs exhibited terrific colloidal stability and a strongly enhanced MR contrast effect compared with the previous results. Quite interestingly, the particle size of the biocompatible Fe_3O_4 NPs could be effectively tuned through a unique gelification effect which is sketched in the lower panel of Fig. 3.¹⁴ Molecular networks could spontaneously form between $Fe(acac)_3$ and HOOC-PEG-COOH with the help of oleylamine, and be accelerated by temperature and time, which reduced the thermal decomposition rate constants of the Fe precursor, consequently altering the particle size. In fact, the strong coordination between the ligands and metal ions is ubiquitous for synthesizing colloidal particles, which always opens up new ways for tuning the particle size or morphology.

3.2 Post surface modification with biocompatible coatings

Non-aqueous synthesis represented by a thermal decomposition method, with the absence of complicated surface binding situations involving water and hydroxyl ions, can yield high quality inorganic NPs with perfect monodispersity, high crystallinity degree, and satisfying size tunability.^{1,4} Adequate surface modifications are essentially required to enable the water soluble, biocompatible, and surface functionalizable NPs for biomedical applications.

Generally, polymers, zwitterionic molecules, and biomolecules are all available as biocompatible coating materials.^{39,79–81} Among all the polymers used for improving the solubility and biocompatibility of NPs, PEG and PEG-copolymers are currently most popular and found to be most effective, and with respect to *in vivo* applications, the improved stealth properties of NPs upon PEGylation are attractive due to their high hydrophilicity, nearly neutral charge, and steric hindrance.^{2,82,83} PEG-based modification of hydrophobic NPs post synthesis can be categorized into two approaches: encapsulation typically by amphiphilic molecules,³⁹ and ligand exchange by coordinating with the anchoring groups.^{18,21,84} Amphiphilic molecule encapsulation is principally based on hydrophobic-hydrophobic interactions between the hydrophobic surface ligand of NPs and the hydrophobic segments of amphiphilic molecules such as PEG-phospholipid, which is quite effective for transferring particles to aqueous phase solution but leaves a hydrophobic layer behind heavily shielding the inorganic core.^{2,4} In contrast, surface ligand exchange determined by the binding affinity of the anchoring group of the biocompatibility ligand to metal ions of NPs is proved to be a reliable approach upon suitable selection of ligands. For example, the PEG ligand carrying two phosphate groups at one end and a maleimide group at the other end, denoted as dp-PEG-mal, was successfully designed by Gao and coworkers, and demonstrated to effectively replace the oleate ligand of $NaGdF_4$ or $NaGdF_4:Yb, Er$ NPs.^{31,85,86} Because of the improved binding affinity to the particle surface, the dp-PEG-mal-coated NPs exhibited long-term colloidal stability in both water and PBS, which endowed the particles with excellent blood circulation behavior in the following *in vivo* applications. Notably, the anchoring groups of surface ligands not only determine the affinity to metal ions, but also tune the physical properties of NPs. For example, iron oxide NPs coated with PEG ligands with different anchoring moieties, *i.e.*, PEG2000 molecule bearing diphosphate (DP), hydroxamate (HX), and catechol (CC) groups, respectively, were found to show different relaxation performances as MRI contrast agents (shown in Fig. 4 and Table 1).⁸⁷

For *in vivo* applications, anti-biofouling properties of the surface coating are indispensable for efficiently directing the NPs to the region of interest. Apart from PEG molecules as outstanding anti-biofouling materials, zwitterions, containing both positively and negatively charged groups but with overall neutral surface charge, are also found to be superior anti-biofouling materials through strong ionic structuring of water and

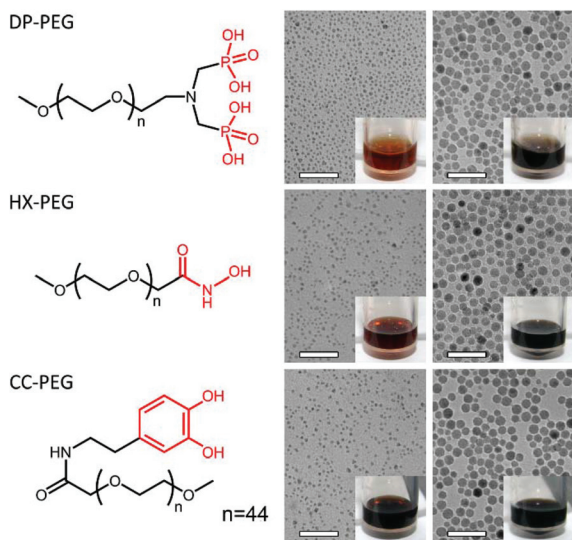


Fig. 4 Chemical structures of three PEG ligands bearing different anchoring groups for post surface modification of the 3.6 nm and 10.9 nm Fe_3O_4 nanoparticles, together with TEM images of the particles and photographs of their aqueous solutions. All embedded scale bars correspond to 50 nm. Reproduced from ref. 87 with permission, copyright 2014, Wiley-VCH.

Table 1 The different relaxivities ($\text{mM}^{-1} \text{s}^{-1}$) and r_2/r_1 of PEGylated Fe_3O_4 nanoparticles. Reproduced from ref. 87 with permission, copyright 2014, Wiley-VCH

	3.6 nm Fe_3O_4 NPs			10.9 nm Fe_3O_4 NPs		
	r_2	r_1	r_2/r_1	r_2	r_1	r_2/r_1
NP@DP-PEG	24.6	3.21	7.69	79.1	3.24	24.4
NP@HX-PEG	48.8	4.2	11.6	92.1	3.12	29.6
NP@CC-PEG	44.8	3.47	12.9	89.7	2.48	36.2

creating a highly hydrophilic surface.^{25,57} Particularly, zwitterionic coating with low molecular weight molecules can endow NPs with good biocompatibility with little apparent increase of the HD size under physiological conditions, which is much larger for PEGylated NPs.^{25,88} This shows great advantages regarding the engineering of rapid-circulating particles for renal clearance as discussed in section 2. Also through the surface ligand exchange process, Bawendi and coworkers reported a 10 nm-sized zwitterionic iron oxide NP using a compact dopamine sulfonate ligand, with good colloidal stability against time, pH (6.0–8.5), and salinity.⁸⁹ It was further shown that the zwitterionic particles had a reduced nonspecific affinity compared to the negatively charged NPs toward serum proteins. Apart from the sulfobetaine derivatives, zwitterions also include amino acids,^{88,90} carboxybetaine derivatives,^{91,92} phosphorylcholine copolymers,⁹³ etc., and can be coated onto the particle surface upon covalent or noncovalent interactions.

Recently, the cell membrane coated NPs have been emerging as a biomimetic and camouflaged platform for *in vivo*

diagnosis and therapy, which consist of a nanoparticulate core coated with a membrane derived from a cell, such as red blood cells (RBC), platelets, macrophage cells, cancer cells or stem cells.^{94–99} The cell membrane translates multiple functional membrane components to the NP surface, thus allowing the NPs to be perceived by the body as the source cell by interacting with its surrounding using the translocated components. Zhang and coworkers reported the functionalized Au NPs with cellular membranes derived directly from natural RBCs, and obtained Au NPs fully enclosed by continuous RBC membranes through extrusion, which endowed the particles with immunosuppressive functionalities for effectively evading macrophage uptake.⁴⁰ Similarly, Fe_3O_4 @RBC NPs were also prepared through the same way to exhibit prolonged circulation time and reduced accelerated blood clearance by function of a “don’t eat me” marker CD47 on the RBC surface.¹⁰⁰ He and coworkers constructed a biomimetic photodynamic therapy (PDT) platform by fusing mesoporous-silica-encapsulated $\beta\text{-NaYF}_4\text{:Yb}^{3+}, \text{Er}^{3+}$ UCL NPs with stem-cell membranes through extrusion, which resulted in long circulation time and tumor-targeting ability for the designed probes.²² Apart from the conventional extrusion strategy, microfluidic electroporation was also demonstrated to facilitate the magnetic NPs to enter into RBC-vesicles, resulting in better colloidal stability and improved *in vivo* MRI and photothermal therapy (PTT) performances.⁶² Same as cell membrane coating, self-peptide is also a shiny biomimetic coating material for biocompatibility and most importantly the “stealthy” properties. It was revealed by Discher’s group that the minimal “self” peptide computationally designed from human CD47 protein delayed macrophage-mediated clearance of NPs, which promoted persistent circulation that enhanced dye and drug delivery to tumors.¹⁰¹ Gao’s group also proved the modification of self-peptide onto the nanoprobe could efficiently delay the clearance of the NPs from the bloodstream.³⁰

3.3 Reproducible synthesis of inorganic NPs

Until now, most NPs reported in the literature have been synthesized through batch preparations. To achieve large-scale production of high quality NPs to fulfill their clinical applications, however, the poor batch-to-batch reproducibility remains hindered, due to the complexity of the nanoparticle formation process especially within the thermal decomposition method involving not only the nucleation and growth processes but also the decomposition of the precursor.¹⁰² Any random variations of reaction parameters would lead to unpredicted effects on the particle size, composition, and size/composition distributions, and further on their physical properties. Fortunately, developing flow chemistry from industrial production of organic compounds to nanoparticle synthesis seems to bring solutions to the reproducibility issue, mainly because of the automatic and continuous synthetic conditions without man-made intervention.^{103,104} In view of the above advantages, flow synthesis has stimulated interest in the preparation of nanomaterials such as semiconductor nanocrystals (CdSe , ZnS , etc.)^{105,106} and metal NPs

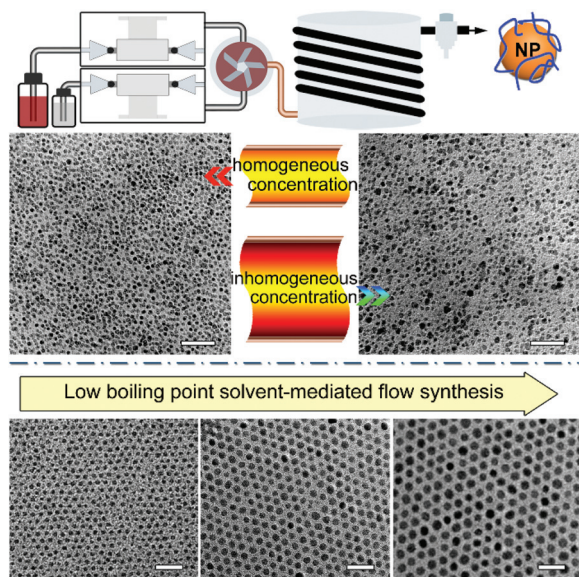


Fig. 5 Sketch of the flow synthetic system for producing biocompatible NPs, together with the representative TEM images of the particles obtained under the impact of monomer concentration inside the tube reactor, and changing the species and concentrations of the low boiling point solvent. The embedded scale bars correspond to 50 nm and 25 nm respectively. Reproduced from ref. 102 and 110 with permission, copyright 2015, American Chemical Society, and copyright 2016, Royal Society of Chemistry, respectively.

(Au, Ag, Ni, *etc.*).^{107–109} Recently, Gao's group reported a flow synthesis of biocompatible Fe_3O_4 NPs with steady quality by utilizing a coil reactor through a one-step reaction, which is illustrated in the upper panel of Fig. 5.¹⁰² The flow parameters including residence time, linear velocity, and tube diameter were tailored for narrowing the particle size distribution, combined with theoretical simulations. It was found out that lowering the linear velocity of the laminar flow narrowed the particle size distribution due to effectively suppressed residence time distribution, but the simultaneously prolonged residence time encouraged Ostwald ripening leading to a reverse tendency for particle size distribution. Most importantly, the effect of the monomer concentration distribution within the tube reactor on the particle size distribution was uncovered for the first time. Accordingly, PEGylated Fe_3O_4 NPs with size distribution sufficiently narrower than that achieved through batch preparation were obtained. Moreover, the resulting 4.6 nm particles exhibited excellent colloidal stability and high longitudinal relaxivity up to $11.1 \text{ mM}^{-1} \text{ s}^{-1}$, manifesting the reliability of flow synthesis of NPs as MRI contrast agents. Based on the flow chemistry, Gao and coworkers also achieved monodisperse magnetic/UCL $\text{NaGdF}_4:\text{Yb,Er}$ NPs with a tunable size in a range of 4–10 nm shown in the lower panel of Fig. 5.¹¹⁰ Benefiting from the high pressure preparative conditions, low boiling point solvents such as cyclohexane and methanol were allowed to be used as a co-solvent with 1-octadecene, which offers flexible room for size tuning without sacrificing

the monodispersity of particle size through reducing the viscosity and/or increasing the solubility of the precursors. Upon further biocompatible surface modification with PEG2000 bearing a biphosphate group, the NPs exhibited a terrific T_1 contrast enhancement effect as well as the UCL, which can be used to construct multimodal imaging probes.

Apart from size control, the composition of multicomponent inorganic NPs can also be tuned through flow synthesis. For example, a continuous production of $\text{Cu}_2\text{ZnSnS}_4$ NPs was reported by Cabot's group, which allowed simple and efficient control of the NP composition over a wide range by adjusting the solution flow rate and an appropriate choice of the precursor concentration.¹⁰⁵ Most importantly, several grams of particles were steadily obtained under open-air conditions, which validated the reliability of flow chemistry for large scale production of high quality NPs. This is highly desirable for their practical applications.

4. Bioconjugation strategies for biocompatible NP-based probes

Targeted recognition attracts increasing interest among diagnosis and therapy of disease based on NPs. Functionalized NPs can be conjugated with biomolecules such as proteins, nucleic acids, peptides and so on for obtaining active targeting nanoprobes. Abundant chemistries upon conjugation between NPs and biomolecules summarized by Sapsford *et al.* provided a comprehensive understanding of the nanoprobe construction.¹¹¹ Generally speaking, the conjugation reaction can be carried out through covalent or noncovalent interactions as briefly shown in Fig. 6.

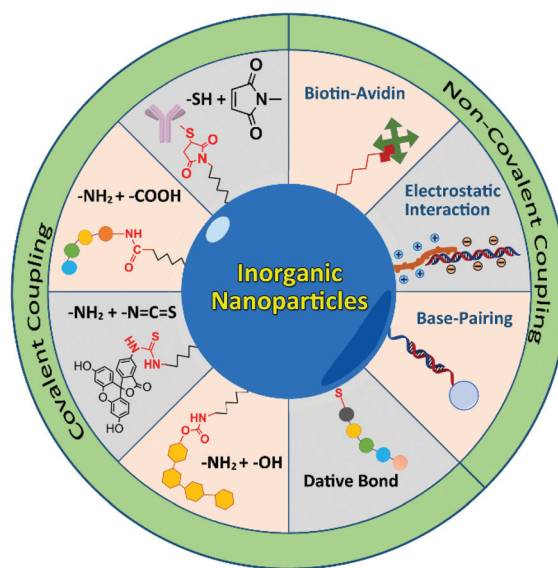


Fig. 6 Brief summarization of the bioconjugation strategies for biocompatible nanoprobes.

4.1 Covalent coupling of biomolecules onto NPs

The surface ligands of NPs terminating with functional groups endow biocompatible NPs with reactive properties, which can be conjugated with biomolecules *via* covalent bonds. The generally used functional groups encompassing $-\text{COOH}$, $-\text{NH}_2$, $-\text{SH}$, and maleimide can be directly or through a cross-linker coupled with biomolecules.

The carboxylic group and primary amino are commonly found in biomolecules, and the amidation reaction between them is often used for the preparation of nanoprobcs. In order to increase the reactivity of $-\text{COOH}$ in aqueous solution, a water-soluble carbodiimide that can form an intermediate compound with the carboxylic moiety is usually involved in mediating the formation of the amide linkages. For example, 1-ethyl-3-(3-dimethylaminopropyl)carbodiimide (EDC) hydrochloride is often used to activate the carboxylic group, together with *N*-hydroxysulfosuccinimide (NHS) or sulfo-NHS which can increase the stability of the active intermediate and thus improve the yield of derivatization.¹¹² PEG-coated Fe_3O_4 NPs with surface reactive carboxyl moieties conjugated with the amino group from an antibody mediated by EDC/sulfo-NHS for obtaining tumor-targeting nanoprobcs were reported by Gao's group.^{75,84,113} Apart from the carboxylic group, isothiocyanate as well as isocyanate compounds can also react with primary amino groups, which occurs rapidly with high selectivity and high yield.¹¹⁴ Rana and Meares found that a monoclonal antibody could be selectively modified only at its N-terminal-amines while leaving lysine amines unmodified using isothiocyanate at pH 7 for maintaining better immunoreactivity.^{115,116}

Mercapto and maleimide groups are another couple of active moieties, and the "click" reaction between them shows very high efficiency. The double bond of maleimide can undergo an alkylation reaction with the mercapto group to form a stable thioether bond at near neutral pH in water.^{117–119} Liu and coworkers used tris(2-carboxyethyl)phosphine hydrochloride (TCEP) to partly reduce the anti-epidermal growth factor receptor monoclonal antibody (anti-EGFR mAb) in order to convert the disulfide groups in the Fc fragments to thiols, and then mixed the (mal-PEG-dp)-coated $\text{NaGdF}_4\text{:Yb,Er}$ particles to construct a tumor specific probe.³¹ Notably, the yield of the "click" reaction approaches 95%. Following a similar strategy, Qiao *et al.* prepared another nanoprobe from the UCL NPs and MGB₂ antibody for gastric cancer imaging.⁸⁵ However, a cross-linker is needed in the coupling reaction between NPs and biological molecules sometimes. For instance, 2-iminothiolane hydrochloride (Traut's Reagent) is a useful reagent for converting primary amines into free sulfhydryl groups, which can easily react with the maleimide group.¹²⁰ Liu and coworkers reported a primary colorectal tumor imaging probe constituted of (mal-PEG-dp)-coated $\text{NaGdF}_4\text{:Yb,Er}$ NPs and jeffamine-modified folic acid (FA) connected by the linker of 2-iminothiolane hydrochloride.¹²¹

In addition, hydroxyl is also considered as a functional group for obtaining conjugates due to a large number of bio-

molecules and ligands containing $-\text{OH}$. Some crosslinkers can easily connect hydroxyl with other functional groups such as amino groups. For example, *N,N'*-carbonyldiimidazole (CDI) is a highly reactive carbonylating agent that contains two acylimidazole leaving groups. It can activate hydroxyl to form an intermediate imidazolyl carbamate with subsequent coupling of amines under non-aqueous conditions. Proteins such as BSA, glucose oxidase, streptokinase, chymotrypsin, dispase, and alkaline phosphatase have been successfully attached to magnetic particles whose surfaces are modified with the amphoteric hydroxyl groups using CDI as a coupling agent.^{122–124}

In some sense, the dative bond, also known as the coordinate bond, is also included in covalent binding interactions, however, it's not as strong as regular covalent bonds and easily effected by pH, oxidation, and other competitive binding ligands. A well-known example is the coordination between Au and sulfhydryl. The sulfur atom of a thiol contributes a lone pair of electrons to the empty orbitals of gold atoms at the interface, which is the predominant basis of Au NPs conjugated with thiolated proteins, peptides, or DNA.¹¹¹

4.2 Noncovalent coupling of biomolecules onto NPs

Noncovalent attachment offering rapid and facile bioconjugation between NPs and biological molecules is also generally used in the preparation of nanoprobcs. Electrostatic interaction is the simplest approach to modify NPs with biomolecules, which depends on the affinity between two oppositely charged species. For example, cetyltrimethylammonium bromide (CTAB)-stabilized Au NPs with high positive charge can adsorb onto the nucleic acids in which the phosphate backbone endows strong negative charge.¹²⁵ The pH value and ionic strength play an important role in the electrostatic interaction between NPs and biomolecules because the hydrolysis or ionization process changes with ambient solvent.^{126,127}

The biotin-avidin system is very useful and versatile, commonly used to conjugate inorganic NPs and a wide range of biomolecules or non-biomolecules including DNA, antibodies, peptides, or fluorescent dyes.^{128–130} The binding between avidin and biotin is extremely stable with an association constant (K_a) of 10^{15} M^{-1} so as to obtain firm bridge-linking not influenced by pH and temperature. Analogue proteins such as neutravidin and streptavidin can replace traditional avidin for higher binding affinity. Gao and coworkers utilized the specific recognition of the streptavidin-biotin pair to prepare a fluorescent probe capable of detecting Epstein-Barr (EB) virus infection in patients' serum samples.¹³¹ Streptavidin was first covalently conjugated with CdTe@dBsa , and then captured by the biotinylated antiIgA antibody which can specifically be recognized by EB virus capsid antigen IgA (VCA-IgA) in serum of nasopharyngeal carcinoma patients. Overall, the biotin-avidin system provides a utility conjugation platform due to the strong affinity and wide selection of bio-reagents, which is an available method to design and construct nanoprobcs for diagnosis.

In addition, other types of noncovalent interactions are involved in the preparation of nanoprobcs, including hydro-

phobic interactions and base-pairing interactions^{132–136} for better serving the *in vitro* detection and *in vivo* diagnosis applications.

5. Biocompatible NP-based *in vivo* imaging

Benefitting from the fast development of preparing techniques of high quality inorganic NPs and the various surface modification and conjugation strategies, biocompatible NPs represent highly promising platforms in the biological and biomedical applications. With respect to *in vivo* applications, many attempts from different fields have been devoted to exploring the applications of NPs in imaging, therapy, and drug delivery. Recently, a lot of reviews have summarized the various biomedical applications of NPs in therapy and drug delivery,^{2,32,41–43,137–140} and in this section we will mainly focus on the recent progress of imaging based on biocompatible NPs, with a special emphasis on atherosclerosis imaging and tumor imaging by active targeting and tumor microenvironment stimuli-responsive ones.

5.1 Atherosclerosis imaging

Cardiovascular disease is one of the leading causes of death worldwide, and the morbidity and mortality increase year by year. Atherosclerosis is a major component of cardiovascular disease, and differentiating vulnerable plaques from stable plaques remains challenging in the clinic. Recently, Qiao *et al.* exploited a macrophage specific upconversion molecular probe to distinguish the vulnerable atherosclerotic plaques.¹⁴¹ Osteopontin (OPN), a secreted biomarker associated with macrophages and foamy macrophages, was selected as the target for identifying the vulnerable plaques. *In vivo* imaging studies and *ex vivo* immunohistochemical analysis confirmed that OPN was expressed more in vulnerable atherosclerotic plaques than in stable ones. The resulting UCNP-anti-OPN probe presented excellent optical imaging and MRI results of differentiating vulnerable and stable atherosclerotic plaques as shown in Fig. 7. Wang's group fabricated a second NIR window (NIR-II) Ag₂S-PEG@ICG nanoprobe for sensitive atherosclerosis imaging, in which the lipophilicity of the C18 chain to the atherosclerosis microenvironment benefited the selective accumulation of probes in the region of atherosclerosis plaques. The high spatial resolution NIR-II fluorescence

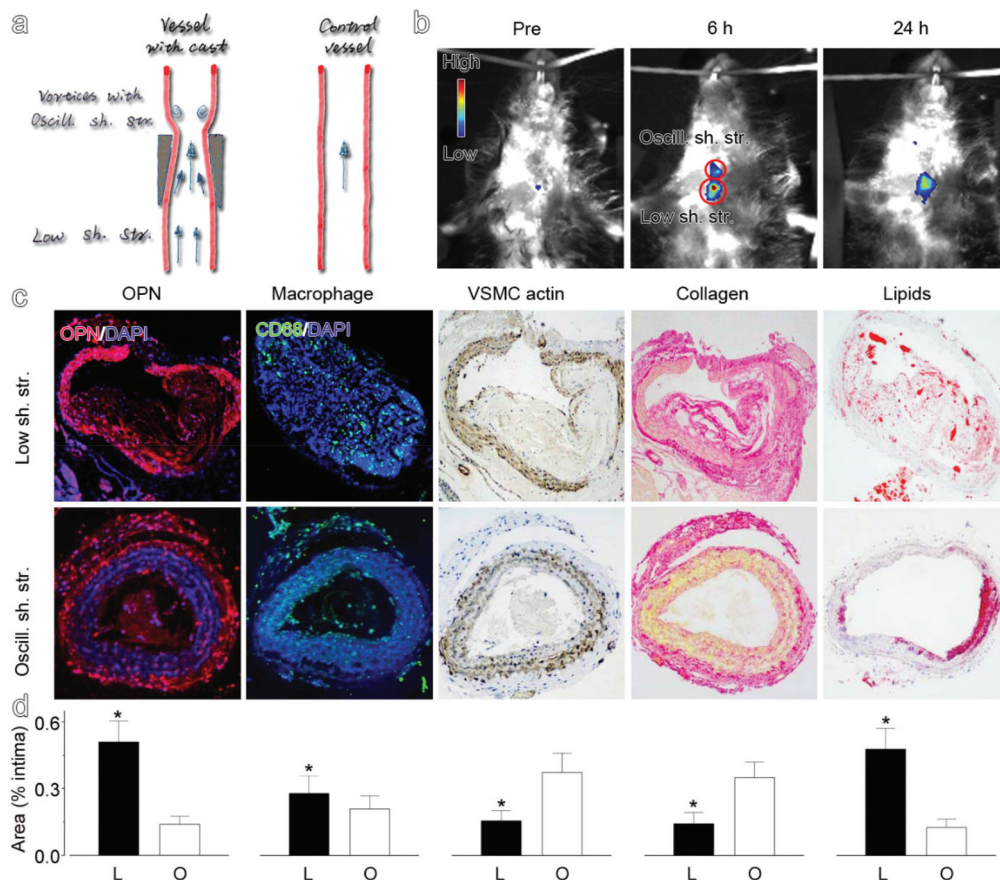


Fig. 7 (a) Schematic drawing for showing the varied stress-induced plaques in ApoE^{-/-} mouse, (b) *in vivo* UCL images based on the UCLNP-anti-OPN probe (the region of interest is encircled with red circles for showing the oscillatory shear stress (top) and the lowered shear stress region (bottom) of the constrained vessel), (c) histological analyses, and (d) quantified data of the different plaque regions upon various staining (**P* < 0.05). Reproduced from ref. 141 with permission, copyright 2017, American Chemical Society.

imaging of Ag₂S QDs combining with real-time PA imaging of ICG proved the feasibility of the nanoprobe for atherosclerosis targeting in an ApoE^{-/-} mouse model.¹⁴²

5.2 Active tumor targeting imaging

Unprecedented progress has been made in the diagnosis of many diseases based on nanoprobe, especially various forms of cancer. NPs can be preferentially accumulated in the tumor area by the enhanced permeation and retention (EPR) effect due to the disordered and leaky tumor vasculatures and poor lymphatic drainage. Tumors can be detected in this passive targeted manner, however, the uptake of NPs not only strongly depends on the particle size, shape, and surface coating, but also is highly related to the tumor microenvironment.^{27,143,144} For instance, gastric and pancreatic cancers show an insufficient EPR effect due to certain characteristics of the tumor microenvironment, including hypovascularity and thick fibrosis.¹⁴⁴ Therefore, developing an active targeting imaging strategy is urgent for the sensitive detection of tumors.

With the fast developments of molecular biology, it is found that the onset and progression of various diseases, especially for cancer, are highly correlated with the aberrant activities of certain biological molecules.^{145–147} Various biomarkers, enzyme-responsive substrates, disease targets and corresponding target ligands have been discovered, which promotes the active targeting molecular imaging technique-based nanotechnology widely used in the area of biomedicine. Active targeting methods function on the basis of the specific binding between biomolecules on the surface of NPs and the surface receptors of diseased cells. Therefore, the selection of suitable specific bioligands is essentially pivotal for constructing the targeting nanoprobe. Antibodies, peptides, protein, aptamers, or small molecules (FA and hyaluronic acid) are typically used in *in vivo* imaging to increase the accumulation of NPs into tumor sites on account of the biological differences between diseased and normal tissues.^{31,121,148–150}

Through utilizing tumor-specific antibody mediated recognition, Gao's group developed a series of tumor targeted probe-based NPs for realizing tiny tumor detection.^{31,85,86} Three sized PEGylation NaGdF₄ NPs (5.4 nm, 15.1 nm, and 19.8 nm) were conjugated with anti-EGFR mAb, which can specifically bind to EGFR overexpressed in most solid tumors through a “click reaction” *via* the surface maleimide ending group of the dp-PEG-mal ligand.⁸⁶ As shown in Fig. 8, the *in vivo* imaging results revealed satisfactory tumor-specific targeting ability and strong MR contrast enhancement effects for intraperitoneal xenografts of human colorectal cancer, and the probes presented greatly enhanced tumor uptake efficacies in comparison with the mother particles, by a factor of nearly four. Furthermore, MRI and UCL dual-modality nanoprobe was established based on NaGdF₄:Yb,Er NPs.³¹ Through the rational design of the probe, tiny tumors of 1.7 mm × 1.9 mm could be clearly visualized in optical imaging, and the MRI results were in good accordance with UCL ones, which improved the detection accuracy. Furthermore, they syn-

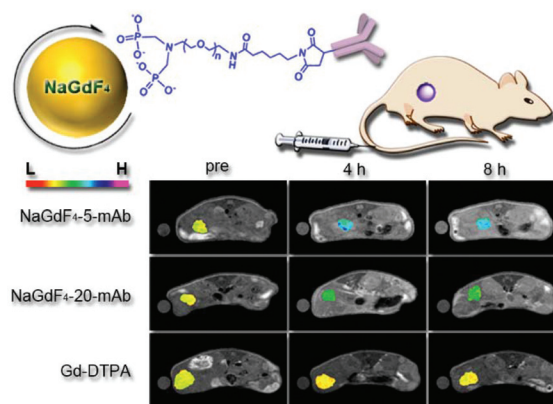


Fig. 8 Illustration of the synthesis of the NaGdF₄ nanoprobe for tumor imaging, and T₁-weighted MR images of tumor-bearing mice acquired before and at different time points based on NaGdF₄-5 and NaGdF₄-20 nanoprobe, and Gd-DTPA, respectively. Reproduced from ref. 86 with permission, copyright 2013, American Chemical Society.

thesized a gastric tumor targeted probe by conjugation of the anti-gastric cancer antibody MGB₂ with NaGdF₄:Yb, Er@NaGdF₄ NPs, and then built a reliable orthotopic gastric cancer mice model that enabled the occurrence of lymphatic metastasis.⁸⁵ Tumor targeting ability was confirmed by UCL imaging and MRI, and lymphatic micrometastasis smaller than 1 mm, and omentum lymph node metastasis could optically be detected. Conde *et al.* also developed a highly sensitive probe for *in vivo* tumor detection on account of the recognition between EGFR and anti-EGFR mAb.¹⁵¹ The 90 nm gold NPs were surrounded by a Raman reporter, encapsulated and entrapped by the PEG polymer and mAb, and the resulting nanoantennas presented a high Raman signal both in cancer cells and in mice bearing xenograft tumors.

Tumor-specific small molecular ligands such as FA and arginine-glycine-aspartate (RGD) peptide are also widely used for enhancing the accumulation of nanoprobe in the tumor site. Their “small size” can increase the loading amounts of targets on the nanocarriers. Liu *et al.* chose FA, a high affinity ligand for folic receptor overexpressed in colorectal tumor, to prepare the nanoprobe.¹²¹ There were nearly 500 FA molecules attached on the surface of one UCL NP. The high payload of targeting molecules together with the outstanding optical properties of core-shell UCL NPs enabled the probe to sensitively visualize the primary colorectal tumor in the complicated intestinal tract. Chen *et al.* reported a dual tumor targeting probe constituted of dye labelled-Au nanoclusters and cyclic RGD together with aptamer AS1411 (Apt).¹⁴⁸ Cyclic RGD is specific to α_vβ₃ integrins overexpressed on the surface of tumors, and Apt is of high affinity to nucleolin overexpressed in the cytoplasm and nucleus of tumor cells. The dual targeting probes exhibited a higher uptake of NPs revealing a higher tumor targeting ability in *in vivo* fluorescent imaging.

Up to now, various functional inorganic nanomaterial-based active targeting probes have been applied in the *in vivo* tumor imaging and therapy.²⁷ However, the major obstacle is

the poor uptake efficiency of the nanoprobe to the tumor site even through the active targeting delivery strategy (less than 10% ID g^{-1}). The ability of target binding of the active probes is of some dispute, for example, most studies show that targeting ligands increase the total accumulation of NPs in the tumor, while some studies can't observe the increasing total accumulation but instead show influence on the distribution within the tumor tissue.^{27,152} In fact, the specific ligand-receptor interaction alone does not necessarily ensure that the nanoprobe could be effectively delivered to the lesion. To manipulate the nanobiointerface interplay between the NPs and biological environment remains the main issue of concern for the nanoprobe design.

5.3 Stimuli-responsive tumor imaging

Researchers gradually realize that the tumor microenvironment is strongly correlated with the growth, invasion, and metastasis of malignant tumor.^{84,153,154} For example, the aberrant physicochemical features such as the overexpressed proteases destroy extracellular matrix integrity and correlate with an advanced tumor stage, while the reduced pH and lowered oxygen pressure are critical to the initiation and maintenance of tumorigenesis.^{84,153-157} Therefore, developing noninvasive methods for visualizing the tumor microenvironment is critical for tumor diagnostics, therapy, and prognostics. Tremendous studies have been devoted to design stimuli-responsive and intelligent nanoprobe for tumor and microenvironment imaging.

5.3.1 Tumor microenvironment imaging. As is known, tumors are heterogeneous due to the dynamics and the diversity of the tumor microenvironment.¹⁵⁸ Acquiring the detailed information of different regions of tumor is helpful for diagnosis and therapy. Commonly, tumor microenvironment imaging can be realized *via* the signal changes, such as optical, MRI, PA, and so on, caused by tumor environmental characteristics including overexpressed proteins, acid, redox, hypoxic surrounding, which allow us to gain a new perspective on tumor-specific detection and imaging.^{84,159-164}

Normally, matrix metalloproteinases (MMPs) occur in the unactivated zymogen form, whereas they are activated and upregulated in almost all types of human cancers.^{164,165} Liu's group reported a novel activatable PA imaging nanoprobe for *in vivo* detection of cancer-related MMPs for the first time.¹⁶⁴ CuS NPs with strong NIR absorbance were conjugated with a red-light-absorbing dye, black hole quencher 3 (BHQ3), *via* a MMP cleavable peptide. The obtained CuS-peptide-BHQ3 probes exhibited strong PA signals at 680 nm and 930 nm before enzyme cleavage owing to the absorption of BHQ3 and CuS NPs, respectively. Once the probes encountered MMPs in tumor areas, free BHQ3 would be released and washed out from the tumor, and the PA signal at 680 nm quickly diminished. The PA signal ratio of 680 nm/930 nm could thus serve as an indicator of MMP activity inside the tumor. The *in vivo* PA imaging results demonstrated that the designed probe could be used for the detection of a specific enzyme activity.

The tumor microenvironment is also characterized by abnormal extracellular pH resulting from anaerobic glycolysis, typically in a range of 6.2–6.9 and slightly lower than that for normal tissues (7.2–7.4).^{154,166,167} A protease-activated pH-sensitive fluorescent “off to on” probe for imaging the pH of subcutaneous tumor xenografts shown in Fig. 9 was reported by Hou *et al.*⁸⁴ The targeted probe was constructed based on biocompatible Fe₃O₄ nanocrystals and a ratiometric fluorescent dye (ANNA), and a peptide substrate of MMP-9 as a linker between them to act as a “switch” to control the off and on state of ANNA. The *in vitro* cell imaging results revealed that the fluorescence of the probe could be effectively activated because MMP-9 cleaved the peptide linker to destroy the fluorescence resonance energy transfer (FRET) between the chromophore (ANNA) and the quencher (Fe₃O₄ particles). *In vivo* animal imaging studies revealed that the probe rapidly responded to the MMP-9 expressed in tumor, and further semiquantitative analysis suggested that the current probe could be used for realizing sensitive pH mapping of the tumor microenvironment for visualizing the heterogeneity of tumors with respect to pH.

Apart from abnormal protease expression and pH, hypoxia is also a characteristic feature among most solid tumors due to the imbalance between rapid cancer cell proliferation and limited oxygen supply.^{156,159,168} Shi's group reported an oxygen nanosensor for selectively and reversibly detecting the level of hypoxia both *in vitro* and *in vivo*.¹⁷⁶ They encapsulated the UCL NPs and the oxygen indicator ([Ru(dpp)₃]²⁺Cl₂) into mesoporous silica. The blue emission of the UCL NPs was used to excite the oxygen-sensing dyes. The UCL NP-based nanosensor exhibited sensitive oxygen-responsive imaging within living cells as well as in zebrafish. Jiang's group developed a hypoxia-specific optical nanosensor which was a kind of co-micelle comprising of poly(ϵ -caprolactone)-*b*-poly(*N*-vinylpyrrolidone) (PCL-PVP) and PVP-conjugated iridium(III) complex (Ir-PVP), for *in vivo* cancer metastasis tracking.¹⁵⁹ The NIR phosphorescence emission of Ir-PVP could be activated in the hypoxic microenvironment, and the *in vivo* experimental results revealed that the probe could not only visualize the hypoxia distribution of the tumor region, but also effectively detect the metastasis of cancer cells to the lungs through the bloodstream or to the lymph node *via* lymphatics.

5.3.2 Tumor microenvironment stimuli-responsive imaging. Traditional diagnosis of tumor based on nanoprobe suffers from some shortcomings, such as a low signal to noise ratio and low sensitivity, limited targeting efficiency, and interference by the complex environment in different types of cancers, which limit their applications to diagnose tumors universally. Recently, motivated by the advanced surface engineering of NPs and the profound understanding of nano-bio interfaces, stimuli-responsive strategies provide new opportunities for improving the performance of the nanoprobe-targeted imaging and therapy. With a rational stimuli-responsive design, the nanomaterials are manipulated spatiotemporally to accumulate at tumor sites *via* interacting with various microenvironment physicochemical aspects, *i.e.*,

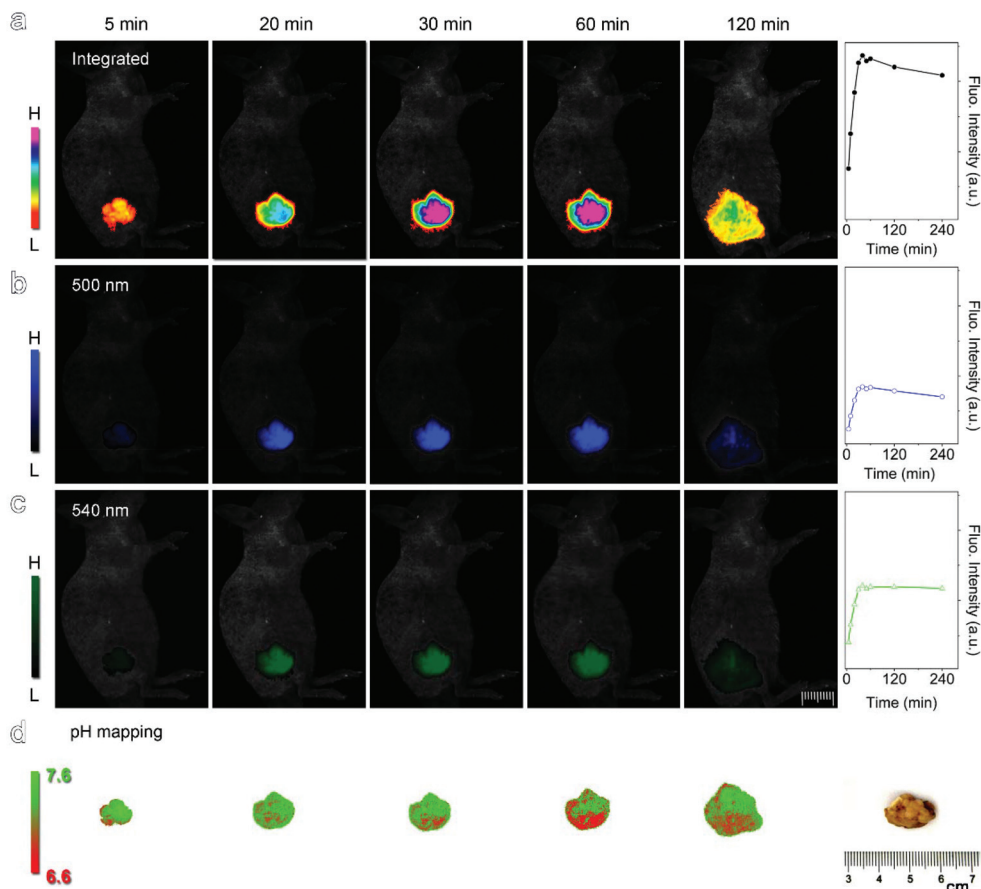


Fig. 9 Color-coded fluorescence images of tumor-bearing mice based on emission of 500–600 nm (a), 500 nm (b), and 540 nm (c), with temporal variations of the integrated optical intensity lying aside. (d) pH mapping of the tumor region with an optical image of the harvested tumor placed at the right-hand side. Reproduced from ref. 84 with permission, copyright 2015, American Chemical Society.

enzymes,^{169–171} pH,^{172–174} redox,^{175,176} which induce structural changes of the nanoprobe and in consequence alter the detection signals and then improve the imaging outcome.

FRET is generally involved to design activatable optical imaging nanoprobe to amplify or boost imaging signals only in response to the tumor sites. Wang's group developed a pH-activatable fluorescence/MRI dual-modality FA-targeted imaging nanoprobe by coencapsulating MnO NPs and coumarin-545 T with a silica shell.¹⁷⁷ The fluorescence of coumarin-545 T was originally quenched by MnO NPs, while would be recovered due to the dissolution of MnO NPs in an acidic tumor environment. Meanwhile, the releasing Mn²⁺ showed an obvious T_1 contrast enhancement in MR imaging of the tumor cell. Yan and coworkers reported a dual-stimuli-responsive and reversibly activatable theranostic nanoprobe for precise tumor-targeting imaging and fluorescence-guided PTT.¹⁷⁸ Cyanine served as a photothermal agent owing to the reversible pH-responsive NIR absorption and fluorescence as well as acting as a tumor-specific imaging signal. Glycosyl functionalized gold nanorods were conjugated with cyanine through MMP-specific peptide as a linker for achieving a MMP/pH synergistically and reversibly activatable theranostic nanoprobe. The as-prepared probes showed tumor-targeted

optical imaging with high specificity and negligible backgrounds. More importantly, an ultra-strong photothermal effect made the probes exhibit tremendous potential in theranostics application. Hu's group reported a Co²⁺-induced coordination self-assembly of luminescent GSH-modified Au NPs for *in vivo* pH-stimuli fluorescence imaging.¹⁷⁹ The fluorescence of the Au clusters was partly quenched when the Au aggregated caused by the coordination between Co²⁺ and the thiol group of GSH modified Au NPs. While in a slightly acidic microenvironment of the tumor, the assembled structure would be disintegrated, and the fluorescence regained.

The above-mentioned “off to on” switchable probes responded to the specific factors at the tumor site are beneficial for improving signal to noise ratios and overcoming the false positive imaging results.

Another kind of nanoprobe manifests as enhancing the original signals or changing the types of detection signals of the tumor region upon the stimulus from the tumor microenvironment. An intelligent pH-triggered fabrication of Au nanoprobe for tumor PA imaging and PTT was reported by Tang's group.¹³⁷ Complementary single-strand DNAs with pyridine-2-imine-terminating groups were modified on the surface of Au NPs, respectively. Alpha-cyclodextrin (α -CD) can encircle

pyridine-2-imine to prevent hybridization of DNA strands on Au NPs under neutral pH. When the nanoprobe reached the tumor area, α -CD was separated from the ends of DNA due to the protonation of pyridine-2-imine in the decreased pH. Consequently, Au NPs self-aggregated through complementary base pairing. The *in vivo* results indicated that the obtained probes could act as an efficient agent for tumor-targeted PA imaging and PTT. Gao and coworkers designed a legumain-triggered aggregatable Au NPs for enhanced PA imaging and retention of chemotherapeutics in brain tumors.¹⁸⁰ The surface of Au NPs was modified with Ala-Ala-Asn-Cys-Lys (Au-AK) and 2-cyano-6-amino-benzothiazole (Au-CABT), respectively. In the presence of legumain, a click cycloaddition reaction occurred between 1,2-thiolamino groups on hydrolyzed Au-AK and the cyano group on Au-CABT, which caused the aggregation of Au NPs. Doxorubicin (DOX) was further loaded on Cy5.5 labelled Au NPs through a pH-sensitive linker. The obtained probes could not only enhance the retention of NPs in glioma cells for sensitive *in vivo* tumor detection by fluorescence and PA imaging, but also showed a positive pre-clinical significance in improving the therapeutic outcome of glioma with reduced systemic toxicity of DOX. Wen *et al.* reported a novel ultrasmall biocompatible WO_{3-x} nanodot for PA/CT imaging and therapy of tumor. WO_{3-x} nanodots could act as a potential radiosensitizer, and show a strong pH/ O_2 -responsive localized surface plasmon resonance (LSPR) in the NIR region. Such properties were well aligned with the weakly acidic and hypoxic microenvironment of tumors. Thus, WO_{3-x} nanodots revealed enhanced PA imaging of tumor with the combination of excellent PTT and radiotherapy.¹⁸¹

Recently, Gao's group reported another tumor microenvironment induced aggregation of magnetic nanoprobe for enhanced T_2 -weighted MR imaging as shown in Fig. 10.³⁰ They designed a GSH-responsive $^{99\text{m}}\text{Tc}$ -labeled Fe_3O_4 nanoprobe with active targeting (RGD-targeted) and dual modality imaging capacities. Dp-PEG-mal was used to coat the NPs

through the diphosphate group, and the remaining maleimide group was used to covalently attach RGD peptide and the self-peptide linked through a disulfide bond. As we know, GSH is highly abundant in tumor regions, and once the disulfide bond was cleaved by GSH, the adjacent NPs will be crosslinked through the "click" reaction between the maleimide residues and mercapto group. The *in vivo* MRI results revealed that the T_2 value of the tumor site could decrease nearly 50% at 8 h post-injection, while the T_2 value of the control group only gave rise to a decrement of 18%. Hyeon and coworkers reported pH-responsive T_1 -weighted MR imaging of tumor based on the disassembly of magnetic nanogrenades triggered by the acidic pH of the tumor microenvironment.¹⁸² The magnetic nanogrenades were prepared *via* chlorin e6 (Ce6) labelled amphiphilic diblock copolymer-assisted self-assembly of small iron oxide NPs. The imidazole on the polymer served as an ionizable group to impart pH sensitivity to the tumor microenvironment, and the increased imidazole ionization in acidic pH led to the surface charge of polymers reversing and polymers swelling, which made nanogrenades disassemble into separated NPs in the tumor site. The obtained nanogrenades showed a pH-responsive T_1 -weighted MRI contrast effect, fluorescence, and PTT activity in *in vivo* tumor treatment. Liu *et al.* reported a tumor microenvironment redox/pH/ H_2O_2 responsive multistage and multifunctional nanoplatform.¹⁸³ MnO_2 NPs stabilized by BSA are encapsulated by coordination polymer shells constructed using *c,c,t*-(diamminedichlorodisuccinato)Pt(IV), hafnium (Hf) ions, and a chemoradiotherapy drug. High-Z element Hf ions can serve as a radio-sensitizer owing to the strong X-ray attenuation capability of Hf to enhance radiotherapy. MnO_2 can trigger the decomposition of tumor endogenous H_2O_2 to produce O_2 , which can overcome the hypoxia-associated resistance of therapy. Meanwhile, within the acidic tumor microenvironment, the decomposition of MnO_2 to release Mn^{2+} could enhance the T_1 contrast effect in MRI. The multifunctional biodegradable theranostics nano-

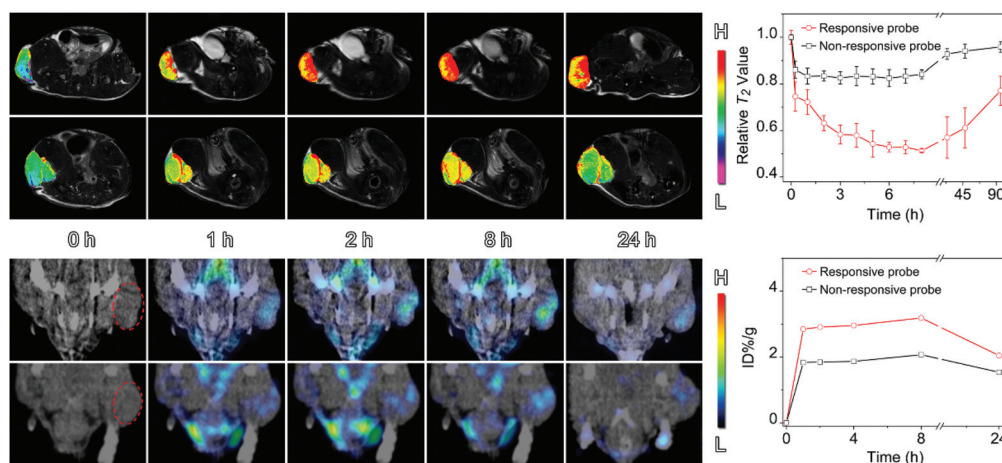


Fig. 10 T_2 -Weighted MRI and SPECT/CT images of tumor-bearing mice injected with the responsive probe and the control probe, respectively, together with corresponding T_2 values and the γ -signal of the tumorous areas respectively. Reproduced from ref. 30 with permission, copyright 2017, Wiley-VCH.

platform not only enabled tumor specific imaging, but also exhibited a satisfactory therapeutic effect *in vivo*. Xu's group also reported a pH-ultrasensitive Mn-based layered double hydroxide (Mn-LDH) NPs for tumor T_1 -weighted MRI.¹⁸⁴ The obtained Mn-LDH exhibited an ultrasensitive pH response and enhanced T_1 imaging for at least 2 days *in vivo*.

Apart from the reinforcing of the MRI effect, intelligent nanoprobes with the T_1 - T_2 switchable MRI contrast effect have also been designed for tumor imaging. By means of the degradation of hyaluronic acid (HA) by hyaluronidase (HAase), a tumor-associated enzyme, Chen's group developed a HAase-responsive aggregation of Fe_3O_4 NPs for *in vivo* tumor MR imaging, which exhibited transition between T_1 and T_2 relaxation character.¹⁸⁵ Ultrasmall Fe_3O_4 NPs coated with HA were first prepared, which showed obvious T_1 relaxation. However upon the degradation of HA on the surface of NPs, the Fe_3O_4 NPs were assembled and exhibited enhanced T_2 relaxation. The *in vitro* results showed that the T_2 signal was enhanced by 36%, and the T_1 signal decreased by 22% in the presence of HAase and acidic environment. Further *in vivo* results revealed that the enzyme-induced self-assembling nanoprobes tuned the T_1 - and T_2 -weighted MRI in the tumor site. Li *et al.* reported a bioeliminable magneto plasmonic nanoassembly constituted by Fe_3O_4 nanoclusters and a gold nanoshell for CT, PA, and MRI trimodal imaging-guided tumor PTT.¹⁶⁹ Superparamagnetic Fe_3O_4 NPs were fabricated into nanoclusters with the mediator of gelatin which could be degraded by MMPs such as MMP-2 and MMP-9. The obtained NPs were collapsed into small ones in response to the tumor local microenvironment of acidic pH and enzyme, and showed obvious transition from the bright T_1 signal to the dark T_2 signal together with enhanced PA and CT imaging effects.

6. Conclusion and outlook

Bearing excellent intrinsic physical properties and versatile surfaces, inorganic NPs have shown great potential for constructing multifunctional nanoprobes for *in vivo* applications covering both imaging and therapy, which in turn raise indispensable requirements for the particles including biocompatibility, colloidal stability and high efficacy. Even though the inorganic NP-based probes for biomedical applications have been investigated for many years, the studies on how they behave *in vivo* especially the pharmacokinetics and unintentionally formed protein corona are still in their infancy, and remain challenging for improving the treatment efficacy. Biocompatibility of NPs has been achieved by either *in situ* coating during the synthesis or post surface modification using various ligands, and biofunctionality can meanwhile be realized by conjugation of biomolecules. Nonetheless, developing reliable strategies for suitable surface coatings to construct specific nanoprobes needs more efforts, because most of the reported NP-based probes have very poor delivery efficiency towards the site of interest. A multi-targeting NP system that consists of two or more targeting stages or stimuli-responsive

targeting moieties represents a promising targeting strategy. The ultimate goal of developing nanomedicine is clinical translation; therefore, sufficient supply of high quality NPs is essential, and flow chemistry emerges as a promising way to achieve large-scale production without sacrificing the NPs' quality, yet the reports on mass production are currently limited and still underway to be further developed for the practical applications of NPs.

Conflicts of interest

There are no conflicts to declare.

Acknowledgements

The authors acknowledge the financial support from the NSFC (21403250, 81771902, 81671754, 81530057, 81471726, 81571746, 81671755), the Natural Science Foundation of Shandong Province of China (ZR2017BB009), and the CAS (2016YZ01, PY-2015-32).

Notes and references

- 1 R. R. Qiao, C. H. Yang and M. Y. Gao, *J. Mater. Chem.*, 2009, **19**, 6274.
- 2 J. Nam, N. Won, J. Bang, H. Jin, J. Park, S. Jung, S. Jung, Y. Park and S. Kim, *Adv. Drug Delivery Rev.*, 2013, **65**, 622.
- 3 L. Jing, S. V. Kershaw, Y. Li, X. Huang, Y. Li, A. L. Rogach and M. Gao, *Chem. Rev.*, 2016, **116**, 10623.
- 4 Z. Gao, T. Ma, E. Zhao, D. Docter, W. Yang, R. H. Stauber and M. Gao, *Small*, 2016, **12**, 556.
- 5 K. Zarschler, L. Rocks, N. Licciardello, L. Boselli, E. Polo, K. P. Garcia, L. De Cola, H. Stephan and K. A. Dawson, *Nanomedicine*, 2016, **12**, 1663.
- 6 S. V. Kershaw, L. Jing, X. Huang, M. Gao and A. L. Rogach, *Mater. Horiz.*, 2017, **4**, 155.
- 7 Y. Wei, X. Mo, P. Zhang, Y. Li, J. Liao, Y. Li, J. Zhang, C. Ning, S. Wang, X. Deng, *et al.*, *ACS Nano*, 2017, **11**, 5915.
- 8 C. Liu, Y. Hou and M. Gao, *Adv. Mater.*, 2014, **26**, 6922.
- 9 L. Jing, K. Ding, S. V. Kershaw, I. M. Kempson, A. L. Rogach and M. Gao, *Adv. Mater.*, 2014, **26**, 6367.
- 10 M. Zhu, G. Nie, H. Meng, T. Xia, A. Nel and Y. Zhao, *Acc. Chem. Res.*, 2013, **46**, 622.
- 11 Y. Liu, X. Zhang, C. Cao, Y. Zhang, J. Wei, Y. j. Li, W. Liang, Z. Hu, J. Zhang, Y. Wei, *et al.*, *Adv. Funct. Mater.*, 2017, 1703771.
- 12 J. Lynch, J. Zhuang, T. Wang, D. LaMontagne, H. Wu and Y. C. Cao, *J. Am. Chem. Soc.*, 2011, **133**, 12664.
- 13 N. Lee and T. Hyeon, *Chem. Soc. Rev.*, 2012, **41**, 2575.
- 14 Q. J. Jia, J. F. Zeng, R. R. Qiao, L. H. Jing, L. Peng, F. L. Gu and M. Y. Gao, *J. Am. Chem. Soc.*, 2011, **133**, 19512.
- 15 X. Cheng, R. Sun, L. Yin, Z. Chai, H. Shi and M. Gao, *Adv. Mater.*, 2017, **29**, 1604894.

- 16 Y. C. Wang, K. C. L. Black, H. Luehmann, W. Y. Li, Y. Zhang, X. Cai, D. H. Wan, S. Y. Liu, M. Li, P. Kim, *et al.*, *ACS Nano*, 2013, **7**, 2068.
- 17 E. Y. Zhao, Z. X. Zhao, J. C. Wang, C. H. Yang, C. J. Chen, L. Y. Gao, Q. Feng, W. J. Hou, M. Y. Gao and Q. Zhang, *Nanoscale*, 2012, **4**, 5102.
- 18 K. Ding, L. H. Jing, C. Y. Liu, Y. Hou and M. Y. Gao, *Biomaterials*, 2014, **35**, 1608.
- 19 J. H. Gao, K. Chen, R. G. Xie, J. Xie, S. Lee, Z. Cheng, X. G. Peng and X. Y. Chen, *Small*, 2010, **6**, 256.
- 20 X. Y. Sun, K. Ding, Y. Hou, Z. Y. Gao, W. S. Yang, L. H. Jing and M. Y. Gao, *J. Phys. Chem. C*, 2013, **117**, 21014.
- 21 J. Huang, Y. Hou, C. Liu, L. Jing, T. Ma, X. Sun and M. Gao, *Chem. Mater.*, 2015, **27**, 7918.
- 22 C. Gao, Z. Lin, Z. Wu, X. Lin and Q. He, *ACS Appl. Mater. Interfaces*, 2016, **8**, 34252.
- 23 R. A. Sperling and W. J. Parak, *Philos. Trans. R. Soc., A*, 2010, **368**, 1333.
- 24 R. Bilan, F. Fleury, I. Nabiev and A. Sukhanova, *Bioconjugate Chem.*, 2015, **26**, 609.
- 25 K. P. García, K. Zarschler, L. Barbaro, J. A. Barreto, W. O'Malley, L. Spiccia, H. Stephan and B. Graham, *Small*, 2014, **10**, 2516.
- 26 D. Bobo, K. J. Robinson, J. Islam, K. J. Thurecht and S. R. Corrie, *Pharm. Res.*, 2016, **33**, 2373.
- 27 B. R. Smith and S. S. Gambhir, *Chem. Rev.*, 2017, **117**, 901.
- 28 N. Feliu, D. Docter, M. Heine, P. del Pino, S. Ashraf, J. Kolosnjaj-Tabi, P. Macchiarini, P. Nielsen, D. Alloyeau, F. Gazeau, *et al.*, *Chem. Soc. Rev.*, 2016, **45**, 2440.
- 29 Z. Lin, N. A. Monteiro-Riviere and J. E. Riviere, *Wiley Interdiscip. Rev.: Nanomed. Nanobiotechnol.*, 2015, **7**, 189.
- 30 Z. Y. Gao, Y. Hou, J. F. Zeng, L. Chen, C. Y. Liu, W. S. Yang and M. Y. Gao, *Adv. Mater.*, 2017, **29**, 1701095.
- 31 C. Y. Liu, Z. Y. Gao, J. F. Zeng, Y. Hou, F. Fang, Y. L. Li, R. R. Qiao, L. Shen, H. Lei, W. S. Yang, *et al.*, *ACS Nano*, 2013, **7**, 7227.
- 32 Y. Dai, C. Xu, X. Sun and X. Chen, *Chem. Soc. Rev.*, 2017, **46**, 3830.
- 33 B. Wang, X. He, Z. Zhang, Y. Zhao and W. Feng, *Acc. Chem. Res.*, 2013, **46**, 761.
- 34 E. Blanco, H. Shen and M. Ferrari, *Nat. Biotechnol.*, 2015, **33**, 941.
- 35 D. Docter, S. Strieth, O. Hayden, M. Y. Gao, S. K. Knauer and R. H. Stauber, *Nanomedicine*, 2015, **10**, 503.
- 36 M. Mahmoudi, N. Bertrand, H. Zope and O. C. Farokhzad, *Nano Today*, 2016, **11**, 817.
- 37 Z. Li, L. Wei, M. Y. Gao and H. Lei, *Adv. Mater.*, 2005, **17**, 1001.
- 38 A. S. Karakoti, S. Das, S. Thevuthasan and S. Seal, *Angew. Chem., Int. Ed.*, 2011, **50**, 1980.
- 39 G. Palui, F. Aldeek, W. Wang and H. Mattoussi, *Chem. Soc. Rev.*, 2015, **44**, 193.
- 40 W. Gao, C.-M. J. Hu, R. H. Fang, B. T. Luk, J. Su and L. Zhang, *Adv. Mater.*, 2013, **25**, 3549.
- 41 T. Kang, F. Li, S. Baik, W. Shao, D. Ling and T. Hyeon, *Biomaterials*, 2017, **136**, 98.
- 42 S. Kaur, C. Prasad, B. Balakrishnan and R. Banerjee, *Biomater. Sci.*, 2015, **3**, 955.
- 43 L. Zhu and V. P. Torchilin, *Integr. Biol.*, 2013, **5**, 96.
- 44 Y. Sun, W. Feng, P. Yang, C. Huang and F. Li, *Chem. Soc. Rev.*, 2015, **44**, 1509.
- 45 S. A. Love, M. A. Maurer-Jones, J. W. Thompson, Y. S. Lin and C. L. Haynes, in *Annual Review of Analytical Chemistry*, eds. R. G. Cooks and E. S. Yeung, 2012, vol. 5, pp. 181.
- 46 J. X. Li, X. L. Chang, X. X. Chen, Z. J. Gu, F. Zhao, Z. F. Chai and Y. L. Zhao, *Biotechnol. Adv.*, 2014, **32**, 727.
- 47 M. Mahmoudi, H. Hofmann, B. Rothen-Rutishauser and A. Petri-Fink, *Chem. Rev.*, 2012, **112**, 2323.
- 48 A. Gnach, T. Lipinski, A. Bednarkiewicz, J. Rybka and J. A. Capobianco, *Chem. Soc. Rev.*, 2015, **44**, 1561.
- 49 R. D. Brohi, L. Wang, H. S. Talpur, D. Wu, F. A. Khan, D. Bhattarai, Z. U. Rehman, F. Farmanullah and L. J. Huo, *Front. Pharmacol.*, 2017, **8**, 606.
- 50 M. Z. Ahmad, B. A. Abdel-Wahab, A. Alam, S. Zafar, J. Ahmad, F. J. Ahmad, P. Midoux, C. Pichon and S. Akhter, *J. Nanosci. Nanotechnol.*, 2016, **16**, 7873.
- 51 O. T. Bruns, T. S. Bischof, D. K. Harris, D. Franke, Y. Shi, L. Riedemann, A. Bartelt, F. B. Jaworski, J. A. Carr, C. J. Rowlands, *et al.*, *Nat. Biomed. Eng.*, 2017, **1**, 0056.
- 52 M. Zhou, J. J. Li, S. Liang, A. K. Sood, D. Liang and C. Li, *ACS Nano*, 2015, **9**, 7085.
- 53 Q. J. He, Z. W. Zhang, F. Gao, Y. P. Li and J. L. Shi, *Small*, 2011, **7**, 271.
- 54 C. Zhou, M. Long, Y. P. Qin, X. K. Sun and J. Zheng, *Angew. Chem., Int. Ed.*, 2011, **50**, 3168.
- 55 G. D. Zhang, Z. Yang, W. Lu, R. Zhang, Q. Huang, M. Tian, L. Li, D. Liang and C. Li, *Biomaterials*, 2009, **30**, 1928.
- 56 K. Ding, J. Zeng, L. Jing, R. Qiao, C. Liu, M. Jiao, Z. Li and M. Gao, *Nanoscale*, 2015, **7**, 11075.
- 57 J. B. Liu, M. X. Yu, X. H. Ning, C. Zhou, S. Y. Yang and J. Zheng, *Angew. Chem., Int. Ed.*, 2013, **52**, 12572.
- 58 Z. W. Li, C. Wang, L. Cheng, H. Gong, S. N. Yin, Q. F. Gong, Y. G. Li and Z. Liu, *Biomaterials*, 2013, **34**, 9160.
- 59 H. S. Choi, B. I. Ipe, P. Misra, J. H. Lee, M. G. Bawendi and J. V. Frangioni, *Nano Lett.*, 2009, **9**, 2354.
- 60 W. Guo, X. Sun, O. Jacobson, X. Yan, K. Min, A. Srivatsan, G. Niu, D. O. Kiesewetter, J. Chang and X. Chen, *ACS Nano*, 2015, **9**, 488.
- 61 X. D. Zhang, D. Wu, X. Shen, P. X. Liu, F. Y. Fan and S. J. Fan, *Biomaterials*, 2012, **33**, 4628.
- 62 L. Rao, B. Cai, L.-L. Bu, Q.-Q. Liao, S.-S. Guo, X.-Z. Zhao, W.-F. Dong and W. Liu, *ACS Nano*, 2017, **11**, 3496.
- 63 H. Arami, A. Khandhar, D. Liggitt and K. M. Krishnan, *Chem. Soc. Rev.*, 2015, **44**, 8576.
- 64 S. G. Elci, Y. Jiang, B. Yan, S. T. Kim, K. Saha, D. F. Moyano, G. Yesilbag Tonga, L. C. Jackson, V. M. Rotello and R. W. Vachet, *ACS Nano*, 2016, **10**, 5536.

- 65 S. T. Kim, K. Saha, C. Kim and V. M. Rotello, *Acc. Chem. Res.*, 2013, **46**, 681.
- 66 S. Hirn, M. Semmler-Behnke, C. Schleh, A. Wenk, J. Lipka, M. Schaffler, S. Takenaka, W. Moller, G. Schmid, U. Simon, *et al.*, *Eur. J. Pharm. Biopharm.*, 2011, **77**, 407.
- 67 R. R. Arvizo, O. R. Miranda, D. F. Moyano, C. A. Walden, K. Giri, R. Bhattacharya, J. D. Robertson, V. M. Rotello, J. M. Reid and P. Mukherjee, *PLoS One*, 2011, **6**, e24374.
- 68 H. S. Choi, W. Liu, P. Misra, E. Tanaka, J. P. Zimmer, B. I. Ipe, M. G. Bawendi and J. V. Frangioni, *Nat. Biotechnol.*, 2007, **25**, 1165.
- 69 X. W. Liang, H. L. Wang, Y. Zhu, R. Zhang, V. C. Cogger, X. Liu, Z. P. Xu, J. E. Grice and M. S. Roberts, *ACS Nano*, 2016, **10**, 387.
- 70 H. L. Ma, Y. F. Xu, X. R. Qi, Y. Maitani and T. Nagai, *Int. J. Pharm.*, 2008, **354**, 217.
- 71 K. Saha, M. Rahimi, M. Yazdani, S. T. Kim, D. F. Moyano, S. Hou, R. Das, R. Mout, F. Rezaee, M. Mahmoudi, *et al.*, *ACS Nano*, 2016, **10**, 4421.
- 72 M. Kopp, S. Kollenda and M. Epple, *Acc. Chem. Res.*, 2017, **50**, 1383.
- 73 S. J. Liu, Y. C. Han, R. R. Qiao, J. F. Zeng, Q. J. Jia, Y. L. Wang and M. Y. Gao, *J. Phys. Chem. C*, 2010, **114**, 21270.
- 74 L. H. Jing, C. H. Yang, R. R. Qiao, M. Niu, M. H. Du, D. Y. Wang and M. Y. Gao, *Chem. Mater.*, 2010, **22**, 420.
- 75 F. Q. Hu, L. Wei, Z. Zhou, Y. L. Ran, Z. Li and M. Y. Gao, *Adv. Mater.*, 2006, **18**, 2553.
- 76 F. Q. Hu, Z. Li, C. F. Tu and M. Y. Gao, *J. Colloid Interface Sci.*, 2007, **311**, 469.
- 77 S. J. Liu, B. Jia, R. R. Qiao, Z. Yang, Z. L. Yu, Z. F. Liu, K. Liu, J. Y. Shi, O. Y. Han, F. Wang, *et al.*, *Mol. Pharm.*, 2009, **6**, 1074.
- 78 J. Zeng, B. Jia, R. Qiao, C. Wang, L. Jing, F. Wang and M. Gao, *Chem. Commun.*, 2014, **50**, 2170.
- 79 A. V. Kroll, R. H. Fang and L. F. Zhang, *Bioconjugate Chem.*, 2017, **28**, 23.
- 80 R. H. Fang, Y. Jiang, J. C. Fang and L. Zhang, *Biomaterials*, 2017, **128**, 69.
- 81 Y. I. Park, Y. Piao, N. Lee, B. Yoo, B. H. Kim, S. H. Choi and T. Hyeon, *J. Mater. Chem.*, 2011, **21**, 11472.
- 82 H. Bin Na, I. S. Lee, H. Seo, Y. I. Park, J. H. Lee, S. W. Kim and T. Hyeon, *Chem. Commun.*, 2007, **48**, 5167.
- 83 Y. M. Huh, Y. W. Jun, H. T. Song, S. Kim, J. S. Choi, J. H. Lee, S. Yoon, K. S. Kim, J. S. Shin, J. S. Suh, *et al.*, *J. Am. Chem. Soc.*, 2005, **127**, 12387.
- 84 Y. Hou, J. Zhou, Z. Y. Gao, X. Y. Sun, C. Y. Liu, D. H. Shangguan, W. S. Yang and M. Y. Gao, *ACS Nano*, 2015, **9**, 3199.
- 85 R. R. Qiao, C. H. Liu, M. H. Liu, H. Hu, C. Y. Liu, Y. Hou, K. C. Wu, Y. N. Lin, J. M. Liang and M. Y. Gao, *ACS Nano*, 2015, **9**, 2120.
- 86 Y. Hou, R. R. Qiao, F. Fang, X. X. Wang, C. Y. Dong, K. Liu, C. Y. Liu, Z. F. Liu, H. Lei, F. Wang, *et al.*, *ACS Nano*, 2013, **7**, 330.
- 87 J. Zeng, L. Jing, Y. Hou, M. Jiao, R. Qiao, Q. Jia, C. Liu, F. Fang, H. Lei and M. Gao, *Adv. Mater.*, 2014, **26**, 2694.
- 88 W. Wang, A. Kapur, X. Ji, B. Zeng, D. Mishra and H. Mattoussi, *Bioconjugate Chem.*, 2016, **27**, 2024.
- 89 H. Wei, N. Insin, J. Lee, H.-S. Han, J. M. Cordero, W. Liu and M. G. Bawendi, *Nano Lett.*, 2012, **12**, 22.
- 90 A. K. Murthy, R. J. Stover, W. G. Hardin, R. Schramm, G. D. Nie, S. Gourisankar, T. M. Truskett, K. V. Sokolov and K. P. Johnston, *J. Am. Chem. Soc.*, 2013, **135**, 7799.
- 91 W. Yang, S. Liu, T. Bai, A. J. Keefe, L. Zhang, J.-R. Ella-Menye, Y. Li and S. Jiang, *Nano Today*, 2014, **9**, 10.
- 92 L. Zhang, H. Xue, C. L. Gao, L. Carr, J. N. Wang, B. C. Chu and S. Y. Jiang, *Biomaterials*, 2010, **31**, 6582.
- 93 M. Jawanda, B. F. L. Lai, J. N. Kizhakkedathu, K. Ishihara and R. Narain, *Polym. Chem.*, 2013, **4**, 3140.
- 94 Y. Zhai, J. Su, W. Ran, P. Zhang, Q. Yin, Z. Zhang, H. Yu and Y. Li, *Theranostics*, 2017, **7**, 2575.
- 95 X. Ren, R. Zheng, X. Fang, X. Wang, X. Zhang, W. Yang and X. Sha, *Biomaterials*, 2016, **92**, 13.
- 96 M. Xuan, J. Shao, L. Dai, Q. He and J. Li, *Adv. Healthcare Mater.*, 2015, **4**, 1645.
- 97 Z. Wu, T. Li, W. Gao, T. Xu, B. Jurado-Sanchez, J. Li, W. Gao, Q. He, L. Zhang and J. Wang, *Adv. Funct. Mater.*, 2015, **25**, 3881.
- 98 W. Gao and L. Zhang, *J. Drug Targeting*, 2015, **23**, 619.
- 99 J. G. Piao, L. M. Wang, F. Gao, Y. Z. You, Y. J. Xiong and L. H. Yang, *ACS Nano*, 2014, **8**, 10414.
- 100 L. Rao, L.-L. Bu, J.-H. Xu, B. Cai, G.-T. Yu, X. Yu, Z. He, Q. Huang, A. Li, S.-S. Guo, *et al.*, *Small*, 2015, **11**, 6225.
- 101 P. L. Rodriguez, T. Harada, D. A. Christian, D. A. Pantano, R. K. Tsai and D. E. Discher, *Science*, 2013, **339**, 971.
- 102 M. Jiao, J. Zeng, L. Jing, C. Liu and M. Gao, *Chem. Mater.*, 2015, **27**, 1299.
- 103 R. L. Hartman, J. P. McMullen and K. F. Jensen, *Angew. Chem., Int. Ed.*, 2011, **50**, 7502.
- 104 S. Marre and K. F. Jensen, *Chem. Soc. Rev.*, 2010, **39**, 1183.
- 105 A. Shavel, D. Cadavid, M. Ibáñez, A. Carrete and A. Cabot, *J. Am. Chem. Soc.*, 2012, **134**, 1438.
- 106 P. Laurino, R. Kikkeri and P. H. Seeberger, *Nat. Protocols*, 2011, **6**, 1209.
- 107 Z. Huang, H. Jiang, P. Liu, J. Sun, D. Guo, J. Shan and N. Gu, *J. Mater. Chem. A*, 2015, **3**, 1925.
- 108 V. Sebastian, S.-K. Lee, C. Zhou, M. F. Kraus, J. G. Fujimoto and K. F. Jensen, *Chem. Commun.*, 2012, **48**, 6654.
- 109 E. J. Roberts, S. E. Habas, L. Wang, D. A. Ruddy, E. A. White, F. G. Baddour, M. B. Griffin, J. A. Schaidle, N. Malmstadt and R. L. Brutchey, *ACS Sustainable Chem. Eng.*, 2017, **5**, 632.
- 110 M. Jiao, L. Jing, C. Liu, Y. Hou, J. Huang, X. Wei and M. Gao, *Chem. Commun.*, 2016, **52**, 5872.
- 111 K. E. Sapsford, W. R. Algar, L. Berti, K. B. Gemmill, B. J. Casey, E. Oh, M. H. Stewart and I. L. Medintz, *Chem. Rev.*, 2013, **113**, 1904.
- 112 J. V. Staros, R. W. Wright and D. M. Swingle, *Anal. Biochem.*, 1986, **156**, 220.

- 113 R. R. Qiao, Q. J. Jia, S. Huwel, R. Xia, T. Liu, F. B. Gao, H. J. Galla and M. Y. Gao, *ACS Nano*, 2012, **6**, 3304.
- 114 A. Rifai and S. S. Wong, *J. Immunol. Methods*, 1986, **94**, 25.
- 115 T. M. Rana and C. F. Meares, *Bioconjugate Chem.*, 1990, **1**, 357.
- 116 T. M. Rana and C. F. Meares, *J. Am. Chem. Soc.*, 1990, **112**, 2457.
- 117 M. D. Partis, D. G. Griffiths, G. C. Roberts and R. B. Beechey, *J. Protein Chem.*, 1983, **2**, 263.
- 118 G. Gorin, P. A. Martic and G. Doughty, *Arch. Biochem. Biophys.*, 1966, **115**, 593.
- 119 D. G. Smyth, O. O. Blumenfeld and W. Konigsberg, *Biochem. J.*, 1964, **91**, 589.
- 120 R. Jue, J. M. Lambert, L. R. Pierce and R. R. Traut, *Biochemistry*, 1978, **17**, 5399.
- 121 C. Y. Liu, Y. F. Qi, R. R. Qiao, Y. Hou, K. Y. Chan, Z. Q. Li, J. Y. Huang, L. H. Jing, J. Du and M. Y. Gao, *Nanoscale*, 2016, **8**, 12579.
- 122 Z. M. Saiyed, S. Sharma, R. Godawat, S. D. Telang and C. N. Ramchand, *J. Biotechnol.*, 2007, **131**, 240.
- 123 M. Koneracká, P. Kopčanský, M. Timko, C. N. Ramchand, A. de Sequeira and M. Trevan, *J. Mol. Catal. B: Enzym.*, 2002, **18**, 13.
- 124 R. V. Mehta, R. V. Upadhyay, S. W. Charles and C. N. Ramchand, *Biotechnol. Tech.*, 1997, **11**, 493.
- 125 X. M. Miao, X. Ning, Z. B. Li and Z. Y. Cheng, *Sci. Rep.*, 2016, **6**, 32358.
- 126 A. Vincent, S. Babu, E. Heckert, J. Dowding, S. M. Hirst, T. M. Inerbaev, W. T. Self, C. M. Reilly, A. E. Masunov, T. S. Rahman, *et al.*, *ACS Nano*, 2009, **3**, 1203.
- 127 S. Patil, A. Sandberg, E. Heckert, W. Self and S. Seal, *Biomaterials*, 2007, **28**, 4600.
- 128 M. Wilchek and E. A. Bayer, *Trends Biochem. Sci.*, 1989, **14**, 408.
- 129 M. Wilchek and E. A. Bayer, *Anal. Biochem.*, 1988, **171**, 1.
- 130 N. M. Green, *Adv. Protein Chem.*, 1975, **29**, 85.
- 131 Y. Li, L. Jing, K. Ding, J. Gao, Z. Peng, Y. Li, L. Shen and M. Gao, *RSC Adv.*, 2014, **4**, 22545.
- 132 A. P. Tiwari, S. J. Ghosh and S. H. Pawar, *Anal. Methods*, 2015, **7**, 10109.
- 133 C. A. Mirkin, R. L. Letsinger, R. C. Mucic and J. J. Storhoff, *Nature*, 1996, **382**, 607.
- 134 L. L. Li, P. Wu, K. Hwang and Y. Lu, *J. Am. Chem. Soc.*, 2013, **135**, 2411.
- 135 J. Zhang, Y. Fu, Y. Mei, F. Jiang and J. R. Lakowicz, *Anal. Chem.*, 2010, **82**, 4464.
- 136 R. Hu, X. B. Zhang, R. M. Kong, X. H. Zhao, J. H. Jiang and W. H. Tan, *J. Mater. Chem.*, 2011, **21**, 16323.
- 137 Z. Yu, M. Wang, W. Pan, H. Wang, N. Li and B. Tang, *Chem. Sci.*, 2017, **8**, 4896.
- 138 J. N. Liu, W. B. Bu and J. L. Shi, *Chem. Rev.*, 2017, **117**, 6160.
- 139 T. Thambi, J. H. Park and D. S. Lee, *Chem. Commun.*, 2016, **52**, 8492.
- 140 A. Jhaveri, P. Deshpande and V. Torchilin, *J. Controlled Release*, 2014, **190**, 352.
- 141 R. Qiao, H. Qiao, Y. Zhang, Y. Wang, C. Chi, J. Tian, L. Zhang, F. Cao and M. Gao, *ACS Nano*, 2017, **11**, 1816.
- 142 C. Wu, Y. Zhang, Z. Li, C. Li and Q. Wang, *Nanoscale*, 2016, **8**, 12531.
- 143 Z. Cheng, A. Al Zaki, J. Z. Hui, V. R. Muzykantov and A. Tsourkas, *Science*, 2012, **338**, 903.
- 144 M. R. Kano, Y. Bae, C. Iwata, Y. Morishita, M. Yashiro, M. Oka, T. Fujii, A. Komuro, K. Kiyono, M. Kaminishi, *et al.*, *Proc. Natl. Acad. Sci. U. S. A.*, 2007, **104**, 3460.
- 145 E. Simon, *Meas. Sci. Technol.*, 2010, **21**, 112002.
- 146 I. E. Tothill, *Semin. Cell Dev. Biol.*, 2009, **20**, 55.
- 147 R. Weissleder and M. J. Pittet, *Nature*, 2008, **452**, 580.
- 148 X. Sun, Y. Li, T. Liu, Z. Li, X. Zhang and X. Chen, *Adv. Drug Delivery Rev.*, 2017, **110**, 38.
- 149 D. Chen, B. W. Li, S. H. Cai, P. Wang, S. W. Peng, Y. Z. Sheng, Y. Y. He, Y. Q. Gu and H. Y. Chen, *Biomaterials*, 2016, **100**, 1.
- 150 J. C. Li, Y. Hu, J. Yang, P. Wei, W. J. Sun, M. W. Shen, G. X. Zhang and X. Y. Shi, *Biomaterials*, 2015, **38**, 10.
- 151 J. Conde, C. C. Bao, D. X. Cui, P. V. Baptista and F. R. Tian, *J. Controlled Release*, 2014, **183**, 87.
- 152 C. H. Choi, C. A. Alabi, P. Webster and M. E. Davis, *Proc. Natl. Acad. Sci. U. S. A.*, 2010, **107**, 1235.
- 153 B. Davies, J. Waxman, H. Wasan, P. Abel, G. Williams, T. Krausz, D. Neal, D. Thomas, A. Hanby and F. Balkwill, *Cancer Res.*, 1993, **53**, 5365.
- 154 B. A. Webb, M. Chimenti, M. P. Jacobson and D. L. Barber, *Nat. Rev. Cancer*, 2011, **11**, 671.
- 155 D. Yue, Y. Wang, J. Y. Xiao, P. Wang and C. S. Ren, *Asian J. Androl.*, 2009, **11**, 541.
- 156 R. Kumar, E.-J. Kim, J. Han, H. Lee, W. S. Shin, H. M. Kim, S. Bhuniya, J. S. Kim and K. S. Hong, *Biomaterials*, 2016, **104**, 119.
- 157 X. Zheng, X. Wang, H. Mao, W. Wu, B. Liu and X. Jiang, *Nat. Commun.*, 2015, **6**, 5834.
- 158 M. G. Sikkandhar, A. M. Nedumaran, R. Ravichandar, S. Singh, I. Santhakumar, Z. C. Goh, S. Mishra, G. Archunan, B. Gulyas and P. Padmanabhan, *Int. J. Mol. Sci.*, 2017, **18**, 1036.
- 159 X. Zheng, H. Tang, C. Xie, J. Zhang, W. Wu and X. Jiang, *Angew. Chem., Int. Ed.*, 2015, **54**, 8094.
- 160 S. Lee, E. J. Cha, K. Park, S. Y. Lee, J. K. Hong, I. C. Sun, S. Y. Kim, K. Choi, I. C. Kwon, K. Kim, *et al.*, *Angew. Chem., Int. Ed.*, 2008, **47**, 2804.
- 161 R. Weissleder, C. H. Tung, U. Mahmood and A. Bogdanov, *Nat. Biotechnol.*, 1999, **17**, 375.
- 162 X. Z. Ai, C. J. H. Ho, J. Aw, A. B. E. Attia, J. Mu, Y. Wang, X. Y. Wang, Y. Wang, X. G. Liu, H. B. Chen, *et al.*, *Nat. Commun.*, 2016, **7**, 10432.
- 163 K. W. Y. Chan, G. S. Liu, X. L. Song, H. Kim, T. Yu, D. R. Arifin, A. A. Gilad, J. Hanes, P. Walczak, P. C. M. van Zijl, *et al.*, *Nat. Mater.*, 2013, **12**, 268.
- 164 K. Yang, L. Zhu, L. Nie, X. Sun, L. Cheng, C. Wu, G. Niu, X. Chen and Z. Liu, *Theranostics*, 2014, **4**, 134.
- 165 C. Gialeli, A. D. Theocharis and N. K. Karamanos, *FEBS J.*, 2011, **278**, 16.

- 166 L. Wang and C. Li, *J. Mater. Chem.*, 2011, **21**, 15862.
- 167 Y. Wang, K. Zhou, G. Huang, C. Hensley, X. Huang, X. Ma, T. Zhao, B. D. Sumer, R. J. DeBerardinis and J. Gao, *Nat. Mater.*, 2014, **13**, 204.
- 168 J. N. Liu, Y. Liu, W. B. Bu, J. W. Bu, Y. Sun, J. L. Du and J. L. Shi, *J. Am. Chem. Soc.*, 2014, **136**, 9701.
- 169 L. Li, S. Fu, C. Chen, X. Wang, C. Fu, S. Wang, W. Guo, X. Yu, X. Zhang, Z. Liu, *et al.*, *ACS Nano*, 2016, **10**, 7094.
- 170 X. Wang, D. Niu, P. Li, Q. Wu, X. Bo, B. Liu, S. Bao, T. Su, H. Xu and Q. Wang, *ACS Nano*, 2015, **9**, 5646.
- 171 J. Gallo, N. Kamaly, I. Lavdas, E. Stevens, Q. D. Nguyen, M. Wylezinska-Arridge, E. O. Aboagye and N. J. Long, *Angew. Chem., Int. Ed.*, 2014, **53**, 9550.
- 172 R. Ge, M. Lin, X. Li, S. Liu, W. Wang, S. Li, X. Zhang, Y. Liu, L. Liu, F. Shi, *et al.*, *ACS Appl. Mater. Interfaces*, 2017, **9**, 19706.
- 173 L. Zhu, Y. Yang, K. Farquhar, J. Wang, C. Tian, J. Ranville and S. G. Boyes, *ACS Appl. Mater. Interfaces*, 2016, **8**, 5040.
- 174 C. Wang, L. Cheng, Y. Liu, X. Wang, X. Ma, Z. Deng, Y. Li and Z. Liu, *Adv. Funct. Mater.*, 2013, **23**, 3077.
- 175 S. Gao, G. Wang, Z. Qin, X. Wang, G. Zhao, Q. Ma and L. Zhu, *Biomaterials*, 2017, **112**, 324.
- 176 J. N. Liu, Y. Liu, W. B. Bu, J. W. Bu, Y. Sun, J. L. Du and J. L. Shi, *J. Am. Chem. Soc.*, 2014, **136**, 9701.
- 177 B. Y. W. Hsu, M. Ng, A. Tan, J. Connell, T. Roberts, M. Lythgoe, Y. Zhang, S. Y. Wong, K. Bhakoo, A. M. Seifalian, X. Li and J. Wang, *Adv. Healthcare Mater.*, 2016, **5**, 721.
- 178 X. Zhao, C. X. Yang, L. G. Chen and X. P. Yan, *Nat. Commun.*, 2017, **8**, 14998.
- 179 X. Lai, L. Tan, X. Deng, J. Liu, A. Li, J. Liu and J. Hu, *ACS Appl. Mater. Interfaces*, 2017, **9**, 5118.
- 180 S. Ruan, C. Hu, X. Tang, X. Cun, W. Xiao, K. Shi, Q. He and H. Gao, *ACS Nano*, 2016, **10**, 10086.
- 181 L. Wen, L. Chen, S. Zheng, J. Zeng, G. Duan, Y. Wang, G. Wang, Z. Chai, Z. Li and M. Gao, *Adv. Mater.*, 2016, **28**, 5072.
- 182 D. Ling, W. Park, S. J. Park, Y. Lu, K. S. Kim, M. J. Hackett, B. H. Kim, H. Yim, Y. S. Jeon, K. Na and T. Hyeon, *J. Am. Chem. Soc.*, 2014, **136**, 5647.
- 183 J. Liu, Q. Chen, W. Zhu, X. Yi, Y. Yang, Z. Dong and Z. Liu, *Adv. Funct. Mater.*, 2017, **27**, 1605926.
- 184 B. Li, Z. Gu, N. Kurniawan, W. Chen and Z. P. Xu, *Adv. Mater.*, 2017, 1700373.
- 185 H. Zhou, J. Tang, J. Li, W. Li, Y. Liu and C. Chen, *Nanoscale*, 2017, **9**, 3040.